



Mobility & Vehicle Mechanics

*International Journal for Vehicle Mechanics, Engines and
Transportation Systems*

ISSN 1450 - 5304

UDC 621 + 629(05)=802.0

Eid Mohamed	A KINEMATIC ANALYSIS AND EXPERIMENTAL EVALUATION OF THE METAL PUSH BELT CVT	7-26
Saeed Abu Alyzeed Albatlan	PERFORMANCE OF AIR BRAKE COMBINATION VALVE	27-40
Ivan Dunderški	ACTIVE NUMERICAL VEHICLE ACCELERATION CONTROL ALONG ACCELERATION FUNCTION WITH MAXIMUM ENGINE TORQUE EFFICIENCY	41-68
Miroslav Demić Jovanka Lukić Živorad Milić	INVESTIGATION OF VIBRATORY LOADINGS OF MOTOR VEHICLE'S USER IN OPERATIONAL CONDITIONS	69-89



M V M

Mobility Vehicle Mechanics

Editors: Prof. dr Jovanka Lukić; Prof. dr Čedomir Duboka

MVM Editorial Board
University of Kragujevac
Faculty of Engineering
Sestre Janjić 6, 34000 Kragujevac, Serbia
Tel.: +381/34/335990; Fax: + 381/34/333192

Prof. Dr **Belingardi Giovanni**
Politecnico di Torino,
Torino, ITALY

Dr Ing. **Ćučuz Stojan**
Visteon corporation,
Novi Jicin,
CZECH REPUBLIC

Prof. Dr **Demić Miroslav**
University of Kragujevac
Faculty of Engineering
Kragujevac, SERBIA

Prof. Dr **Fiala Ernest**
Wien, OESTERREICH

Prof. Dr **Gillespie D. Thomas**
University of Michigan,
Ann Arbor, Michigan, USA

Prof. Dr **Grujović Aleksandar**
University of Kragujevac
Faculty of Engineering
Kragujevac, SERBIA

Prof. Dr **Knapezyk Josef**
Politechniki Krakowskiej,
Krakow, POLAND

Prof. Dr **Krstić Božidar**
University of Kragujevac
Faculty of Engineering
Kragujevac, SERBIA

Prof. Dr **Mariotti G. Virzi**
Universita degli Studidi Palermo,
Dipartimento di Meccanica ed
Aeronautica,
Palermo, ITALY

Prof. Dr **Pešić Radivoje**
University of Kragujevac
Faculty of Engineering
Kragujevac, SERBIA

Prof. Dr **Petrović Stojan**
Faculty of Mech. Eng. Belgrade,
SERBIA

Prof. Dr **Radonjić Dragoljub**
University of Kragujevac
Faculty of Engineering
Kragujevac, SERBIA

Prof. Dr **Radonjić Rajko**
University of Kragujevac
Faculty of Engineering
Kragujevac, SERBIA

Prof. Dr **Spentzas Constantinos**
N. National Technical University,
GREECE

Prof. Dr **Todorović Jovan**
Faculty of Mech. Eng. Belgrade,
SERBIA

Prof. Dr **Toliskyj Vladimir E.**
Academician NAMI,
Moscow, RUSSIA

Prof. Dr **Teodorović Dušan**
Faculty of Traffic and Transport
Engineering,
Belgrade, SERBIA

Prof. Dr **Veinović Stevan**
University of Kragujevac
Faculty of Engineering
Kragujevac, SERBIA

For Publisher: Prof. dr Miroslav Živković, dean, University of Kragujevac, Faculty of Engineering

***Publishing of this Journal is financially supported from:
Ministry of Education, Science and Technological Development, Republic Serbia***

MVM – International Journal for Vehicle Mechanics, Engines and Transportation Systems
NOTIFICATION TO AUTHORS

The Journal MVM publishes original papers which have not been previously published in other journals. This is responsibility of the author. The authors agree that the copyright for their article is transferred to the publisher when the article is accepted for publication.

The language of the Journal is English.

Journal *Mobility & Vehicles Mechanics* is at the SSCI list.

All submitted manuscripts will be reviewed. Entire correspondence will be performed with the first-named author.

Authors will be notified of acceptance of their manuscripts, if their manuscripts are adopted.

INSTRUCTIONS TO AUTHORS AS REGARDS THE TECHNICAL ARRANGEMENTS OF MANUSCRIPTS:

Abstract is a separate Word document, “*First author family name_ABSTRACT.doc*”. Native authors should write the abstract in both languages (Serbian and English). The abstracts of foreign authors will be translated in Serbian.

This document should include the following: 1) author’s name, affiliation and title, the first named author’s address and e-mail – for correspondence, 2) working title of the paper, 3) abstract containing no more than 100 words, 4) abstract containing no more than 5 key words.

The manuscript is the separate file, „*First author family name_Paper.doc*“ which includes appendices and figures involved within the text. At the end of the paper, a reference list and eventual acknowledgements should be given. References to published literature should be quoted in the text brackets and grouped together at the end of the paper in numerical order.

Paper size: Max 16 pages of B5 format, excluding abstract

Text processor: Microsoft Word

Margins: left/right: mirror margin, inside: 2.5 cm, outside: 2 cm, top: 2.5 cm, bottom: 2 cm

Font: Times New Roman, 10 pt

Paper title: Uppercase, bold, 11 pt

Chapter title: Uppercase, bold, 10 pt

Subchapter title: Lowercase, bold, 10 pt

Table and chart width: max 125 mm

Figure and table title: Figure _ (Table _): Times New Roman, italic 10 pt

Manuscript submission: application should be sent to the following e-mail:

mvm@kg.ac.rs ; lukicj@kg.ac.rs

or posted to address of the Journal:

University of Kragujevac – Faculty of Engineering

International Journal M V M

Sestre Janjić 6, 34000 Kragujevac, Serbia

The Journal editorial board will send to the first-named author a copy of the Journal offprint.

OBAVEŠTENJE AUTORIMA

Časopis MVM objavljuje originalne radove koji nisu prethodno objavljivani u drugim časopisima, što je odgovornost autora. Za rad koji je prihvaćen za štampu, prava umnožavanja pripadaju izdavaču.

Časopis se izdaje na engleskom jeziku.

Časopis *Mobility & Vehicles Mechanics* se nalazi na SSCI listi.

Svi prispeli radovi se recenziraju. Sva komunikacija se obavlja sa prvim autorom.

UPUTSTVO AUTORIMA ZA TEHNIČKU PRIPREMU RADOVA

Rezime je poseban Word dokument, „*First author family name_ABSTRACT.doc*“. Za domaće autore je dvojezičan (srpski i engleski). Inostranim autorima rezime se prevodi na srpski jezik. Ovaj dokument treba da sadrži: 1) ime autora, zanimanje i zvanje, adresu prvog autora preko koje se obavlja sva potrebna korespondencija; 2) naslov rada; 3) kratak sažetak, do 100 reči, 4) do 5 ključnih reči.

Rad je poseban fajl, „*First author family name_Paper.doc*“ koji sadrži priloge i slike uključene u tekst. Na kraju rada nalazi se spisak literature i eventualno zahvalnost. Numeraciju korišćenih referenci treba navesti u srednjim zagradama i grupisati ih na kraju rada po rastućem redosledu.

Dužina rada: Najviše 16 stranica B5 formata, ne uključujući rezime

Tekst procesor: Microsoft Word

Margine: levo/desno: mirror margine; unurašnja: 2.5 cm; spoljna: 2 cm, gore: 2.5 cm, dole: 2 cm

Font: Times New Roman, 10 pt

Naslov rada: Velika slova, bold, 11 pt

Naslov poglavlja: Velika slova, bold, 10 pt

Naslov potpoglavlja: Mala slova, bold, 10 pt

Širina tabela, dijagrama: max 125 mm

Nazivi slika, tabela: Figure __ (Table __): Times New Roman, italic 10 pt

Dostavljanje rada elektronski na E-mail: mvm@kg.ac.rs ; lukicj@kg.ac.rs

ili poštom na adresu Časopisa
Redakcija časopisa M V M
Fakultet inženjerskih nauka
Sestre Janjić 6, 34000 Kragujevac, Srbija

Po objavljivanju rada, Redakcija časopisa šalje prvom autoru jedan primerak časopisa.

Mobility &

Motorna

Vehicle

**Volume 39
Number 2
2013.**

Vozila i

Mechanics

Motori

Eid Mohamed	A KINEMATIC ANALYSIS AND EXPERIMENTAL EVALUATION OF THE METAL PUSH BELT CVT	7-26
Saeed Abu Alyazeed Albatlan	PERFORMANCE OF AIR BRAKE COMBINATION VALVE	27-40
Ivan Dundžerski	ACTIVE NUMERICAL VEHICLE ACCELERATION CONTROL ALONG ACCELERATION FUNCTION WITH MAXIMUM ENGINE TORQUE EFFICIENCY	41-68
Miroslav Demić Jovanka Lukić Živorad Milić	INVESTIGATION OF VIBRATORY LOADINGS OF MOTOR VEHICLE'S USER IN OPERATIONAL CONDITIONS	69-89

Mobility &

Motorna

Vehicle

**Volume 39
Number 2
2013.**

Vozila i

Mechanics

Motori

Eid Mohamed	KINEMATSKA I EKSPERIMENTALNA ANALIZA METALNIH FRIKCIONIH KONTINUALNIH PRENOSNIKA	7-26
Saeed Abu Alyazeed Albatlan	PERFORMANSE VENTILA ZA PRILAGOĐAVANJE SILE KOČENJA VAZDUŠNE KOČNICE	27-40
Ivan Dundžerski	AKTIVNO UPRAVLJANJE UBRZANJEM VOZILA NUMERIČKOM KONTROLOM PO FUNKCIJI UBRZANJA SA MAKSIMALNOM EFEKTIVNOŠĆU MOMENTA MOTORA	41-68
Miroslav Demić Jovanka Lukić Živorad Milić	ISTRAŽIVANJE OSCILATORNIH OPTEREĆENJA KORISNIKA MOTORNIH VOZILA U EKSPLOATACIONIM USLOVIMA	69-89

¹PERFORMANCE OF AIR BRAKE COMBINATION VALVE

Saeed Abu Alyazeed Albatlan

UDC: 629.1; 62.783.52

Summary

In particular, a commercial vehicle may meet critical braking conditions when the vehicle is partially or fully loaded, and when the road is wet or slippery. Under these conditions, the vehicle can spin out, the tractor can jackknife or the trailer can swing out. The air brake system has many design variables; there must be intense research on a method on how to prevent dynamic instability and how to maximize vehicle deceleration. So; some of the commercial vehicles are provided with the combination valve. The behavior of this valve is important to improve the braking performance. In this study, mathematical models and a computer simulation program is used to evaluate the valve and vehicle braking performance characteristics. The measurements performed on the valve using the test rig concord with mathematical model.

Key words: Combination valve, evaluation, performance characteristics, air brake

PERFORMANSE VENTILA ZA PRILAGODAVANJE SILE KOČENJA VAZDUŠNE KOČNICE

UDC: 629.1; 62.783.52

Rezime

Komercijalna vozila moraju da zadovolje uslove kritičnih uslova kočenja kada je vozilo ili potpuno ili delimično opterećeno, i kada je put vlažan ili klizav. U ovakvim uslovima vozilo može da se zanesu, traktor može da se postavi pod uglom prema prikolici ili da se tegljač prevrne. Vazdušni kočni sistem ima puno promenljivih koje treba definisati, te je neophodno uraditi brojna istraživanja da se spreči dinamička nestabilnost i da se maksimizira usporenje vozila. Neka od komercijalnih vozila imaju ventil za prilagođavanje sile kočenja. Poznavanje ponašanja ventila je važno kako bi se poboljšale performanse kočenja. U ovom radu matematički model i računarske simulacije su korišćene za ocenu karakteristika ventila kao i performansi karakteristika kočenja. Merenja izvedena na ventilu su izvedena u saglasnosti a matematičkim modelom.

Ključne reči: ventil za prilagođavanje sile kočenja, ocena, karakteristike performansi, vazдушna konica

¹ *Received January 2013, Revised March 2013, Accepted April 2013*

Intentionally blank

PERFORMANCE OF AIR BRAKE COMBINATION VALVE

*Saeed Abu Alyazeed Albatlan*¹

UDC: 629.1; 62.783.52

1. INTRODUCTION

The brake system is one of the most important systems in a vehicle for its active safety during operation. A brake system must ensure safe control of a vehicle during its normal operation and must bring the vehicle to a smooth stop within the shortest possible distance under emergency conditions [1, 2]. Air brake systems are widely used in commercial vehicles such as trucks, tractor-trailers, and buses. In these brake systems, compressed air is used as energy transmitting medium to actuate the foundation brakes mounted on the axles [3]. An air brake system for truck and trailer combinations comprises a vehicle load sensing valve to control brake pressure of the vehicle axles [4]. A vehicle load responsive brake control device for adjusting the braking force according to the varying load of the vehicle in each braking range; the purpose of the brake control device is to adjust the braking forces in accordance with the dynamic shifting of the axle loads [5]. A load-controlled fluid pressure regulating valve device for tractor-trailer type vehicle brake systems combines in a single housing a unitary piston valve assemblage capable of performing the functions of a relay valve device and a regulating valve device [6]. Combined vehicle antiskid and load-dependent brake control system in digital control of the individual wheel brake pressure regulating valves is provided. These regulating valves may be operated individually or on a per axle basis to vary the brake pressure independent of the operator-controlled brake valve device [7]. For vehicles without electronic control of brake pressure, there is need to vary the control pressure for different load conditions. This is done in order to avoid the instability that would occur if wheels lock (start skidding) in an unsuitable order. This device is called a load sensing valve [8]. In [9] new generations of mechanical and pneumatic load sensing valves are developed with an integrated relay valve and connection to ABS to meet the requirements for modern commercial vehicles. A model is proposed for predicting the pressure transients in the brake chamber of a brake system delivered by a treadle valve [10]. A control scheme for regulating the pressure in the brake chamber is presented [11]. The details of a mathematical model for an air brake system in the presence of leaks can be found in [12]. The complete mathematical models of a relay valve for commercial vehicles are shown in [13].

The aim of the present paper is to evaluate the performance characteristics of the combination valve (Load sensing relay valve). A test rig is built-up and a mathematical modeling and simulation using MATLAB® are used. The model validation is proved by comparing the test results with the simulation results.

¹ Saeed Abu Alyazeed Albatlan, Higher Technological Institute, 10th of Ramadan City, 6th October Branch Cairo, Egypt, Email: saeedzeed@yahoo.com

2. THEORETICAL ANALYSIS

It is important to understand the construction and operation of the combination valve to formulate its mathematical model and to establish the computer simulation program for its operation.

2.1 CONSTRUCTION AND OPERATION OF THE COMBINATION VALVE

Figure 1 shows the various parts of a combination valve. The parts are assembled in the following way as shown in Fig. 2. The operation of brakes takes place when the driver can apply, hold, or release it. Each of these operations is explained in the following phases:

Apply phase, when the brake pedal is pressed, the treadle valve allows the permissible air to flow to combination valve through the input port I. This acts on the primary piston 1, as shown in Fig. 2. This causes the primary piston to move and come into contact with cam rod 2. At this point port of cam rod is closed. During this phase the combined movements of combination lever and cam positions open the valve 3 and the port of cam rod remaining closed. This causes the air moves to charge chamber 6. This closes atmospheric port 4, of valve 5.

Second phase: the pressure in chamber 6, increases to a level where it balances the primary piston force, the inlet valve 3 is closed. During this phase the valve 19 is open. This causes compressed air from the storage reservoir 7, to flow into chamber 17, and wheel brake chamber through 8. This phase is called the hold phase. The pressure of air in the brake chamber reaches a steady value.

Third phase: when the pedal is released the applied force on the primary piston is reduced. This causes air in the chamber 6 to get out as exhaust through cam rod port, at this point valve 3 opens and air from the brake chamber flows to the atmosphere. This phase is called the released phase. This valve is used in tractor on rear axle to adjust the braking forces in accordance with the dynamic shifting of the axle loads.

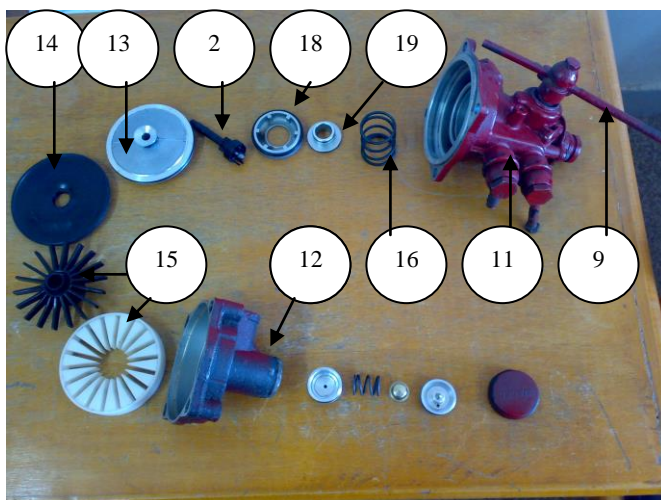


Figure 1 Various parts of combination valve

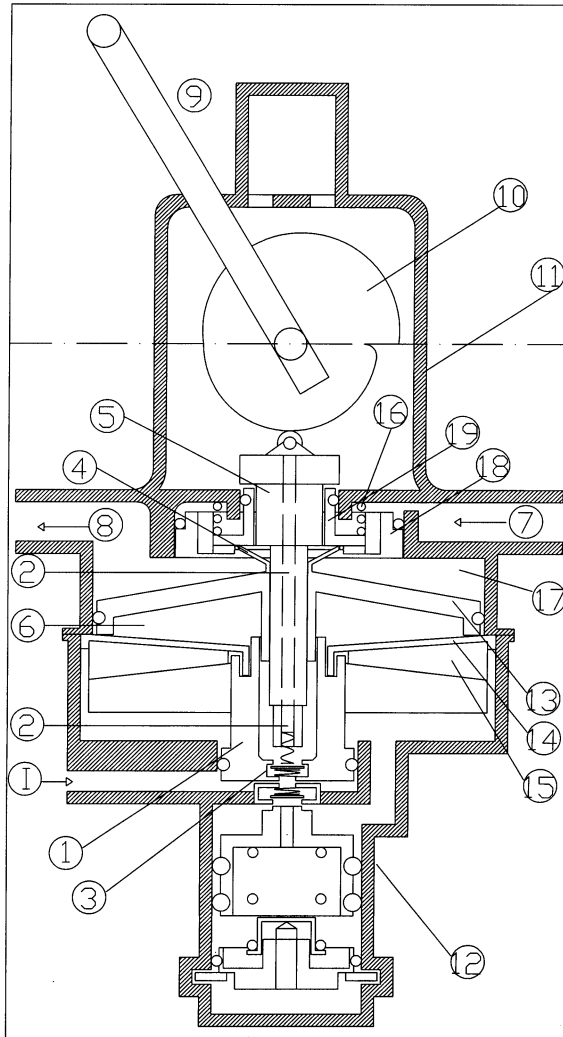


Figure 2: Combination valve construction

1 - Inlet valve port to chamber (A) from treadle valve, 1 - Primary piston, 2 - Cam rod with atmospheric port, 3 - Inlet valve from treadle valve, 4 - Atmospheric control valve, 5 - Regulating rod, 6- Camber (B), 7 - Inlet valve port from reservoir, 8 - Outlet to wheel brake chamber, 9 - Load sensing lever 10-Load sensing Cam, 11- Upper valve body, 12- Lower valve body, 13-Relay piston, 14- Variable area diaphragm, 15- Variable area Diaphragm disc, 16- Coil spring, 17- Chamber (C), 18- Inlet valve seat, 19- Inlet valve from reservoir

2. 2 MATHEMATICAL MODEL

The combination valve mathematical model can be represented in two stages according to air charged in each chamber.

Stage (1)

During apply and hold phases, when the pressure in chamber 6 increases to a level where it balances the primary piston force and the inlet valve 3 is closed.

$$A_A \times P_P = P_B (A_A + A_V), \quad (1)$$

$$P_B = P_P \times \frac{A_A}{(A_A + A_V)}, \quad (2)$$

$$A_V = \frac{A_A (P_P - P_B)}{P_B}, \quad (3)$$

Where are:

- P_B = pressure in chamber 6, bar
- P_P = treadle valve pressure, bar
- A_A = chamber (A) surface area = $784.37 \times 10^{-6} \text{ m}^2$
- A_V = variable area, m^2

Stage (2)

During hold phase, when compressed air from the storage reservoir flows into chamber 17, and brake chamber.

$$P_B \times A_P - F_S = P_C \times A_P, \quad (4)$$

$$P_C = P_B - \frac{F_S}{A_P}, \quad (5)$$

Where:

$$F_S = \text{spring force} = 203 \text{ N}$$

$$P_C = \text{pressure in chamber 17} = \text{wheel brake chamber pressure, bar}$$

$$A_P = \text{primary piston surface area, m}^2$$

Mathematical model of the combination valve constructed on Matlab (Simulink) is shown in Fig. 3. This Figure represents the behavior of valve during operation as follow: Equation (1) is having P_P input and the output is P_B and A_V , where as the input A_A is constant. Equation (2) P_B and P_P represent the input, but A_V represents the output. The output of equation 2 A_V is used to feed the input equation 1 so that the outcome would P_B ,

The second stage P_B and $\frac{F_S}{A_p}$ are the input and the P_C is the output as shown in equations 4 and 5.

3. EXPERIMENTAL WORK

The objective of the experimental work is to test the combination valve under different static load conditions, and to measure the behavior of line pressure brake axels. The experimental data were used for validating the mathematical model results and to evaluate their performance characteristics.

Figure 4 shows a general layout of the test rig, which can be divided, into three main groups: test rig description, the measuring instruments and data acquisition components [DAQ]. The details of each group are given below.

3.1 TEST RIG DESCRIPTION

The test rig is constructed to simulate the vehicle air brake system. The rig uses actual air brake system units and components. It allows testing different types of pressure regulator valves.

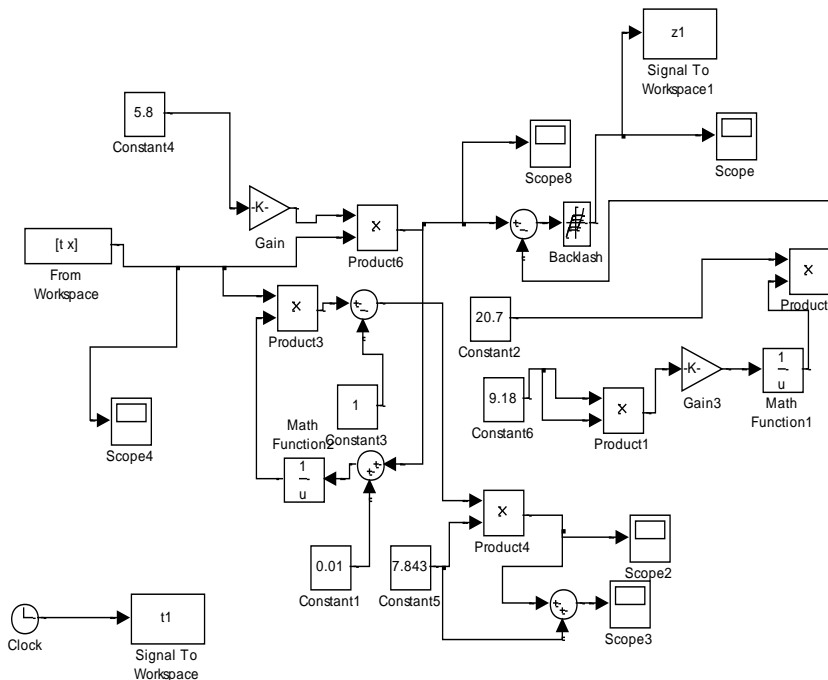
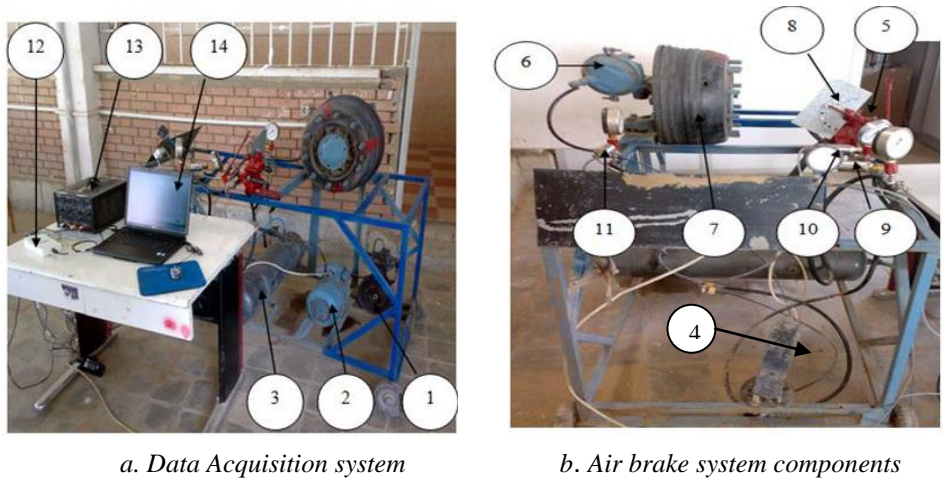


Figure 3 Valve block diagram (Simulink)

The air brake system includes an air compressor 1, coupled with electric motor 2, an air tank 3, brake foot valve (treadle valve) 4, combination valve 5, rear brake chamber 6, rear axle wheel and hoses 7, to connect different components, as shown in Fig. 4 (a,b,c). Air compressor actuating mechanism showed in Fig. 4 consists of electric motor and V- belt connecting air compressor with motor pulley. To have a wide range of rear axle load, the

load sensing lever indexing plate 8, is provide with holes which are corresponding to different loads on the rear axle.



a. Data Acquisition system b. Air brake system components

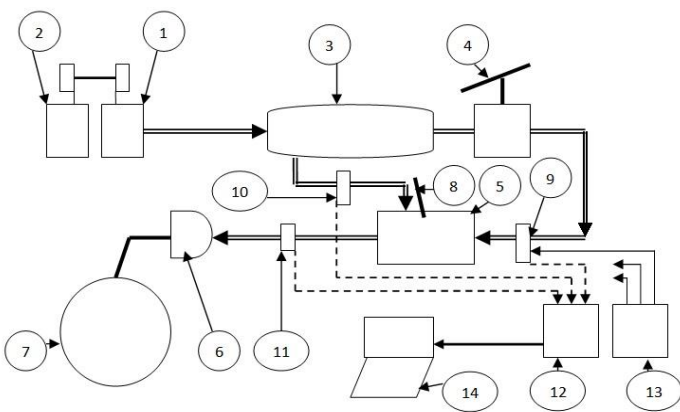


Figure 4 Test rig components and layout

- 1- Air compressor, 2- Electric motor, 3- Air tank , 4- Brake foot valve (treadle valve), 5- Combination valve, 6- Rear brake chamber, 7- Rear axle wheel, 8- Load sensing lever with index plate, 9, 10, 11 – Pressure transducers, 12- Data acquisition board [(A/D) converter], 13- DC supply, 14- CPU

3. 2 THE MEASURING INSTRUMENTS

Test rig is equipped with several measuring instruments, which are necessary for performing the tests. The measuring instruments are shown in Fig. 4, which include:

PRESSURE TRANSDUCERS:

A pressure transducer is mounted at the entrance of each of the combination valve 9, from brake foot valve (treadle valve), entrance to relay valve 10, from the air tank, and output of the relay valve 11, by means of a custom designed and fabricated pitot tube fixture. The purpose of this measurement is to validate the mathematical model results and evaluate their performance characteristics.

3. 3 DATA ACQUISITION COMPONENTS [DAQ]

All the transducers are interfaced with a connector block through shielded cables. The connector block is connected to a DAQ board [14], (connect with computer by USB cable) that collects the data during experimental test runs. This DAQ board can measure (16-channel single ended inputs or 8 channel differential inputs) and can provide two analog output signals. The DAQ board discretizes the analog input signals using an analog-to-digital (A/D) converter 12, and the resulting digital signals are stored in the computer. An application program written in MATLAB / Simulink is used to collect and store the data in the computer [15]. DC supply 13, is used to provide pressure sensors with the required electrical volts. All the transducers are interfaced to a dell-500 computer 14, through an amplifier and signal conditions devices.

4. RESULTS AND DISCUSSION

In this section it is shown clearly that the experiments corroborate the model. Experiments were conducted at different supply pressures for different brake pedal inputs and different cases covering the whole range of load conditions of the vehicle to evaluate the performance of the combination valve.

4. 4 MODEL VALIDATION

The model is validated by comparing experimental results obtained from the test rig undergoing different load conditions with model simulation results. Figures 5 to 7 show the reservoir pressure, treadle valve pressure (relay pressure) and chamber brake line pressure, plotted against the brake time, for experimental and simulation results in different cases covering the whole loading conditions range of the vehicle.

Implementation and tests on a test rig validate the combination valve mathematical model.

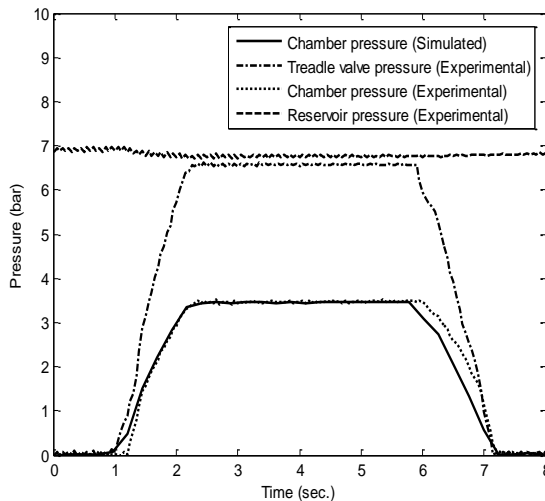


Figure 5: Simulated and experimental air brake pressure at no-load

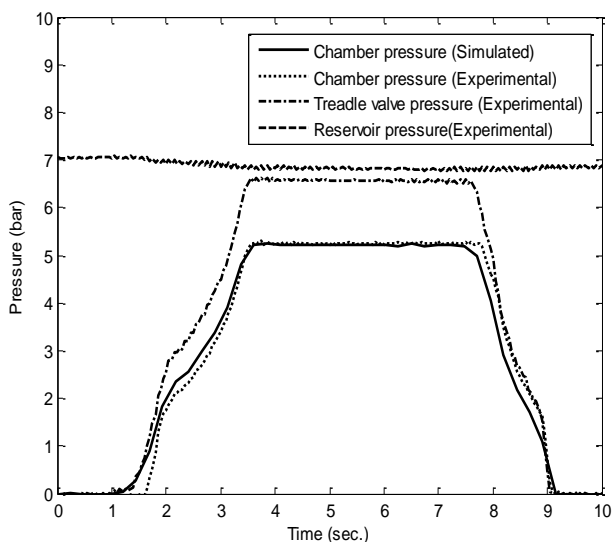


Figure 6 Simulated and experimental air brake pressure at half-load

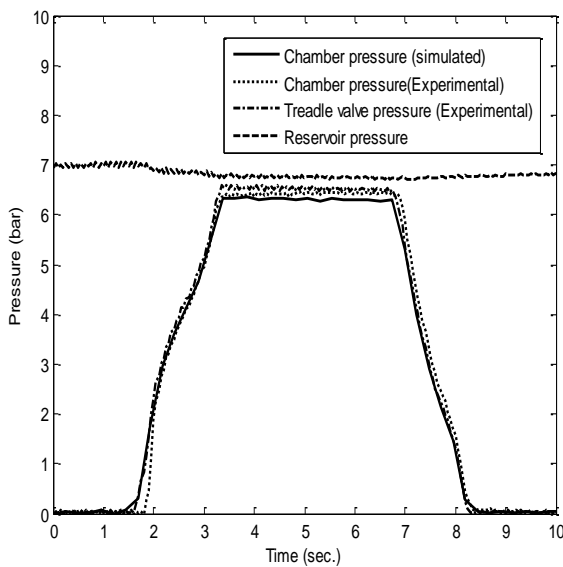


Figure 7 Simulated and experimental air brake pressure at full-load

4. 5 EVALUATING THE PERFORMANCE CHARACTERISTICS OF THE VALVE

Figure 5 represents the behavior of treadle valve pressure, and brake chamber line pressure at no-load, where three phases can be noticed as follows:

Phase (1):

During this phase the brake line pressure increases up to the required pressure whose value depends on the loading condition of the vehicle. This phase is called the apply phase. It depends on pedal travel rate and required braking force.

Phase (2):

The brake line pressure during this phase is constant. This phase is called the hold phase affected by reservoir pressure, relay valve parameters and required braking force.

Phase (3):

This phase is called the released phase, affected by pedal release rate. From Figures 5 to 7 it can be noted that:

The combination valve automatically controls the pressure in brake actuators depending on vehicle load. The distribution of the brake pressure between axle wheels has a large effect on braking performance and vehicle dynamic behavior during braking. Improvement in handling, vehicle stability, stopping distance, and braking efficiency occur due to improved brake balance [16, 17].

4. 6 THE INFLUENCE OF OPERATING PARAMETERS ON VALVE PERFORMANCE

The behavior of combination valve is affected by many factors; among them are the operating parameters. The variation of brake chamber line pressure presented in Figures 8 to 10 is due to load level, and the treadle valve pressure related to pedal rate, show that the treadle valve pressure starts to increase during braking applied. The values of this pressure are affected by the load and pedal rate. This is shown in Figures 5 and 8 respectively.

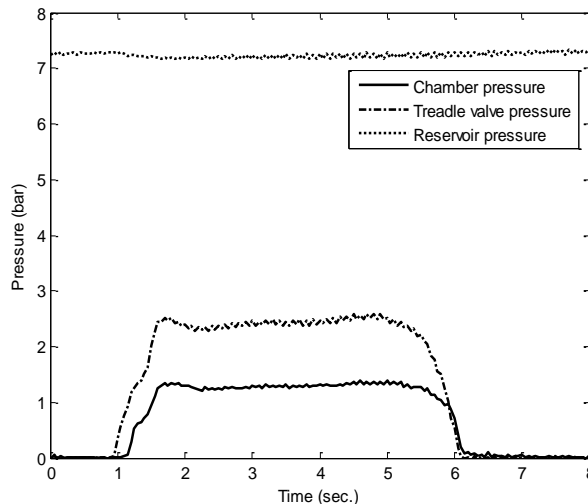


Fig. 8: Experimental result at no-load - part pedal travel

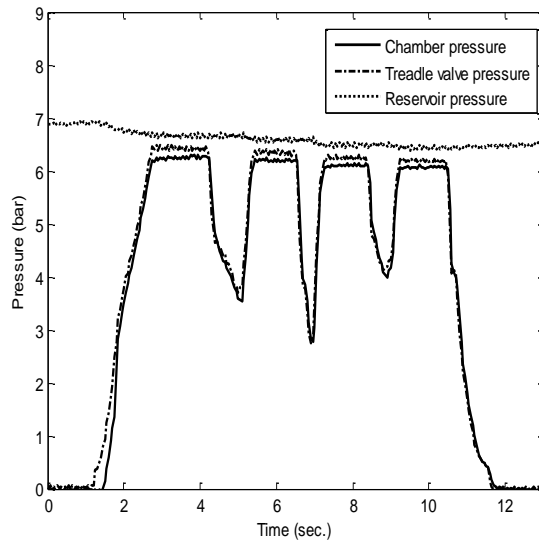


Fig. 9: Experimental result at full- load -variable pedal travel

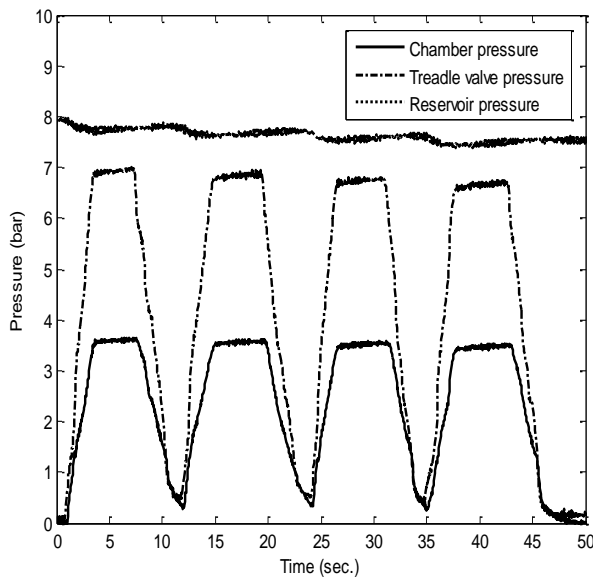


Fig. 10: Experimental result at no-load and fluctuate pedal travel

From figures, 8 to 10 it can be noted that:

- There is a high response for the brake chamber pressure with respect to the treadle valve pressure.

- The brake chamber pressure changes in proportion to loading conditions and treadle valve pressure.
- The treadle valve pressure is regulating valve device for combination valve operation.

5. CONCLUSIONS

- Mathematical models and a computer simulation program is used to evaluate the valve
- The measurements performed on the valve using the test rig concord with mathematical model.

6. REFERENCES

- [1] Garrett, TK., Newton, K., and Steed, W., "The Motor Vehicle", 13rd ed. Warrendale, Pennsylvania: Society of Automotive Engineers, 2001.
- [2] Limpert, R., "Brake Design and Safety", 2nd ed. Warrendale, Pennsylvania: Society of Automotive Engineers, 1999.
- [3] Darbha et al." A Diagnostic System for Air Brakes in Commercial Vehicles", Intelligent Transportation Systems, IEEE Transactions on Volume 7, Issue 3, PP.360 - 376. Sept. 2006.
- [4] Truck and trailer braking systems, Available from: <http://www.freepatentsonline.com/4078844.html>
- [5] Load-dependent braking force control device, Available from: <http://www.patentgenius.com/image/4223955-3.html>
- [6] Vehicle load-controlled brake pressure regulating valve device, Available from: <http://www.patentgenius.com/image/4145089-2.html> Available from:
- [7] Combined antiskid and load-dependent brake control system for a motor vehicle Available from: <http://www.patentgenius.com/patent/4093316.html>
- [8] Brake Calculation Software for Commercial Vehicles. 1998, Available from: <http://www.vehicular.isy.liu.se/>
- [9] Mechanical Load – Sensing Valve with Relay Valve, Available from: http://www.wabcoauto.com/products_and_systems/products-systems-valves
- [10] hankar et al, "Modeling the Pneumatic Subsystem of a S-Cam Air Brake System", Journal of Dynamic Systems, Measurement and Control, Transactions of the ASME, Vol.126, PP. 36-46, March 2004.
- [11] Bowline CL., Subramanian SC., Darbha S., and. Rajagopal KR, "A pressure Control Scheme for Air Brakes in Commercial Vehicles," the IEE Proc. Intelligent Transportation Systems, Vol. 153, Issue 1, pp. 21-32, 2006.
- [12] [Ramaratham, S.](#) "A mathematical model for air brake systems in the presence of leaks," M. Sc. Thesis, Texas A&M University, August, 2008.Available from: <http://handle.tamu.edu/1969.1/86043>
- [13] Shankar et al, "Modeling the Pneumatic Relay Valve of an S-CAM Air Brake System," M. Sc. Thesis, Texas A&M University, May, 2005. Available from: handle/1969.1/2363/etd-tamu-2005A-MEEN-Vilayan.pdf
- [14] National Instruments "Data Acquisition systems," Available from: <http://www.ni.com/digitalio/>

- [15] Johnson, GW. and Jennings, R., "Labview Graphical Programming, 3rd ed. New York: McGraw-Hill, 2008.
- [16] Nosseir et al, "Proper Utilization of Load Sensing Valve to Improve Brake Performance," Ain Shams University. Faculty of Engineering, Vol. 40, No.2, PP. 823-843. June 30, 2005
- [17] Albatlan Saeed Abu Alyazeed, "Air Brake Proportional to Load," International Journal of Modern Engineering Research (IJMER), Vol.2, Issue 4, July-Aug 2012 pp-1898-1902.

¹A KINEMATIC ANALYSIS AND EXPERIMENTAL EVALUATION OF THE METAL PUSH BELT CVT

Eid Mohamed

UDC: 621.839.72

Summary

Most vehicle transmission systems control the ratio between engine speed and wheel speed using a fixed number of metal gears; the Continuously Variable Transmission (CVT) in currently available vehicles utilize a pair of variable-diameter pulleys connected by a belt or chain that can produce an infinite number of engine/wheel speed ratios for improve fuel consumption, drivability effectively, achieve both protection of earth environment and improvement vehicle performance sagging. The present research focuses on developing influence of loading conditions on the slip behavior and torque transmitting ability of the CVT. The model also investigates the range of clamping forces needed to initiate the transmission and to successfully meet the pressure requirements. The experimental setup and the instrumentation are present in detail; the measurement results are presented allowing for a more detailed description of the functional properties of the V-belt type variator, especially those related to reapply value of oil pressure by separate hydraulic unit and reduction ratio.

Keywords: Metal-pushing belt CVT, Friction analysis, Torque transmission, Slip analysis, Experimental analysis.

KINEMATSKA I EKSPERIMENTALNA ANALIZA METALNIH FRIKCIONIH KONTINUALNIH PRENOSNIKA

UDC: 621.839.72

Rezime

Većina sistema za prenos snage vozila upravlja prenosnim odnosom između broja obrtaja motora i brzine točka. Pri čemu se koristi konačan broj zupčanika napravljenih od metala. Sistem kontinualnog prenosa snage (CVT) kod savremenih vozila sastoji se od para kaišnika promjenljivog prečnika povezanih kaišem ili lancem kako bi mogli sa obezbede beskonačan broj stepeni prenosa između broja obrtaja motora i broja obrtaja točka u cilju smanjenja potrošnje goriva, efikasnije vožnje, sa istovremenim pozitivnim efektima na zaštitu okruženja i na poboljšanje performansi vozila. Izloženi rad fokusira se na analizu uticaja uslova opterećenja na klizanje i prenos obrtnog momenta preko CVT. Modelom se analizira opseg sile prethodnog zatezanja neophodnoj za pokretanje sistema i za adekvatno zadovoljenje uslova pritiska. Merni lanac i oprema su detaljno opisani. Eksperimentalni rezultati su prikazani detaljno. Takođe, su opisane radne karakteristike varijatora sa V kaišem, naročito one koje se odnose na hidraulični modul i redukcioni prenos.

Ključne reči: metalni kaišni CVT, frikciona analiza, prenos obrtnog momenta, analiza klizanja, eksperimentalna analiza

¹ Received January 2013, Revised: March 2013, Accepted: April 2013.

Intentionally blank

A KINEMATICS' ANALYSIS AND EXPERIMENTAL EVALUATION OF THE METAL PUSH BELT CVT

Eid Mohamed¹

UDC: 621.839.72

NOMENCLATURE:

LIST OF SYMBOLS

T	The band tension. (The total tension in both band packs.) (N)
F_I	Inertia Force (N)
T_1, T_2	Belt Tensions at ends of the Element (N)
F_c	Centrifugal Force (N)
F_F	Friction force acting between band pack and segment or between neighboring bands (N)
F_N	Total normal force acting on the segment shoulder (N)
F_T	The tangential friction force acting between the pulley surface and the segment side (N)
F_R	Radial friction force acting between the pulley surface and the segment sides (N)
F_{axle}	Axial force acting on the segment (N)
m	Mass of one belt segment (Kg)
V	The velocity of the segment (m/s)
R	The rolling radius of the belt segment (m)
R_{sec}	Radius of the secondary bulley (m)
R_{pr}	Radius of the primary bulley (m)
C	Center distance (m)
β_{pri}	Contact angle for primary pulley (deg)
β_{sec}	Contact angle for secondary pulley (deg)
i_{cvt}	Transmission ratio of CVT (--)
L	Belt Length (m)
P_p, P_s	Primary and secondary oil pressure (N/m ²)
F_s, F_p	Secondary and primary clamping force (N)
A_p, A_s	Primary and secondary pistons area (m ²)
ω_p, ω_s	Primary and secondary pulley velocities (rpm)
x_p, x_s	distance of the primary and secondary pistons (m)
Δx	Initial distance of secondary pulley spring (m)
F_{spr}	Force of secondary pulley spring (N)
C_p, C_s	Primary and secondary pulleys centrifugal coefficient (--)
μ_p, μ_s	Primary and secondary pulley and belt traction coefficient (--)

¹ Eid Mohamed, Automotive and Tractors Engineering, Faculty of Engineering, Helwan University, Cairo, Egypt. Email: Eng_eid74@yahoo.com

LIST OF ACRONYMS:

DCV	Directional Control Valve
CVT	Continuously Variable Transmission
CV	Choke Valves
RMS	Root Mean Square

1. INTRODUCTION**1.1 GENERAL:**

The Continuously Variable Transmission (CVT) is increasingly used in automotive applications. It has an advantage over conventional automatic transmissions, with respect to the large transmission ratio coverage and absence of comfort issues related to shifting events. This enables the engine to operate at more economic operating points. For this reason, CVT equipped cars are more economical than cars equipped with planetary gear automatic transmissions. The key advantages of a CVT that interest vehicle manufacturers and customers can be summarized as:

- Higher engine efficiency.
- Higher fuel economy.
- Smooth acceleration without shift shocks.
- Infinite gear ratios with a small number of parts.
- Easy to manufacture and low cost.
- Light and Compact.

The basic configuration of a metal V-belt CVT consists of two variable diameter pulleys connected by a power-transmitting device i.e. a metal V-belt. The pulley centers are a fixed distance apart. The pulley on the engine side is called the primary or the driver pulley. The other on the final drive (or the wheel side) is the secondary or the driven pulley. Since one of the sheaves on each pulley is movable, the application of an axial force on the movable pulley sheave allows the belt to move radially in the pulley groove. In addition to the radial motion, the belt also moves tangentially around the pulley under the influence of an applied torque. The metal V-belt is made of two series of thin steel bands holding together thin trapezoidal elements. The elements are connected to each other by a system of pegs and holes, a peg in the forward face of an element connected to a hole in the rear face of the element in front. Usually, an initial gap exists between the elements of the belt as they are not tightly pressed together.

Torque is transferred from the driver to the driven pulley by the pushing action of the elements. As the belt moves, an element is carried forward on the driver pulley due to the friction forces generated from the pulley. This forward motion of the element generates compressive forces as it pushes on the element ahead of it. On the driven side, the belt transfers torque to the driven pulley through friction. Due to the presence of friction between the band pack and the elements, the tensile forces in the bands also vary as the belt moves on the driver and driven pulleys. Thus, the operation of such a CVT is based on both the pulling and pushing mechanisms of the composite-structured belt.

1. 2 BACKGROUND OF CVT:

The metal V-belt, manufactured by Van Doorne's Transmission, consists of 400 steel elements and two sets of nine stacked steel bands [1]. The system consists of a primary pulley indirectly linked to the engine through a torque converter and a secondary pulley leading to the final drive gears and wheels. Two pressures, primary and secondary, are associated with the primary and secondary pulleys, respectively. The secondary pressure is the hydraulic supply, or line pressure. The primary pressure is in part dictated by a solenoid relief valve commanded by an electronic engine controller, and is directly related to the difference in primary and secondary pressures. Therefore, our intermediate control objective will be to specify the ratio of primary to secondary pulley speed by means of primary pressure solenoid valve counts. The primary control objective will be to achieve a desired engine speed, which we consider a known function of throttle angle and vehicle speed. We will use this desired engine speed to specify the desired ratio, and then use the desired ratio to specify control input. Thus, back stepping control will be used to achieve our goal. Figure 1 illustrates the basic arrangement of a metal V-belt CVT. The band pack runs over the belt elements, whereas the belt element contacts not only the band pack, but also the pulley sheave.

Continuously variable transmissions (CVTs) are typically composed of two hydraulically actuated variable radii pulleys and a metal pushing belt, the CVTs offer a continuum of infinitely variable gear ratios by changing the location of pulley sheaves. As a result, CVTs have the potential to increase the overall vehicle efficiency and reduce the jerk usually associated with manual and automatic transmissions. One shortcoming, however, is their difficulty in transmitting high torque at low operating speeds, which so far has limited their use to small vehicles. CVT is an emerging automotive transmission technology that offers a continuum of gear ratios between high and low extremes. Today, Continuously Variable Transmissions have lured a great deal of automotive manufacturers and customers. Several car companies like Honda, Toyota, Ford, Nissan, etc., have been doing intensive research to exploit the advantages of a CVT. The chief advantage of a CVT is its ability to offer an infinite range of gear ratios with fewer moving parts, and consequently this influences engine efficiency, fuel economy, and cost.

A sundry of research is available on different aspects of a CVT, e.g. performance, slip behavior, efficiency, configuration design, loss mechanisms, vibrations, etc. Literature pertaining to the slip behavior of a belt CVT will be discussed subsequently. [2] Presented a unified slip theory based on the contributions of creep, compliance, shear deflection, and flexural rigidity of a rubber V-belt. Finite Element Analysis was used to calculate shear deflections in the belt and also to determine the stick-slip conditions on the belt. Incorporated the elastohydrodynamic lubrication theory to model friction between the metal belt and the pulley and also studied, both theoretically and experimentally, the influence of elemental gaps on the slip behavior of belt. The equilibrium conditions were assumed to develop a speed ratio-torque load-axial force relationship. The friction between the band and the elemental block was neglected. It was observed that the gross slip points depend on the torque transmission capacity of the driven side. Performance-based analyses of a metal V-belt drive and obtained a set of equations to describe the belt behavior based on quasi-static equilibrium. Coulomb friction model was used to model friction for all surfaces i.e. among individual bands, band element, and element-pulley. He also studied the deformation and creep of bands and blocks under the influence of torques and forces.

Historically slip in a CVT was regarded as destructive. The reason for this was that slip was not controllable and since it is unstable always resulted in damage to the variator. Recent publications suggest that limited amounts of slip in a push-belt type variator can be allowed [3]. This opens the door to other strategies for lowering the power consumption of CVT's. Not only can slip be used for optimizing variator efficiency actuation efficiency can also be greatly improved. If the safety margin is eliminated, the clamping force can be reduced by more than 25%. This can be directly translated into a 25% decrease in actuation power. Shifting behaviour is also influenced by slip [4]. This effect can be used to greatly reduce the power needed for fast shifting during emergency stopping, tip-shifting and kick down actions. Using this strategy the force needed for shifting is reduced, and with it the power needed from the actuation system is reduced. This has not only effects on the power consumed by the actuation system of the CVT, which is by itself a significant factor in the variator efficiency, but also has some implications on the design of the CVT. If actuation forces are smaller, the actuation system can be smaller and cheaper, and the CVT itself will be lighter. Furthermore, other actuation systems than hydraulics can be considered, for example electromechanical actuation, to further enhance the controllability and efficiency of the actuation system. In this paper, measurements are shown for shifting behaviour of the CVT and a relation will be given with slip in the system. The results are used to model the transient behaviour of the CVT. References [5, 6] analysed the shifting dynamics of a metal V-belt CVT under creep and sliding phases. They proposed a viscoplastic friction model to describe CVT dynamics in creep mode. They also studied the influence of clearance between the elements on the slip behaviour of the belt.

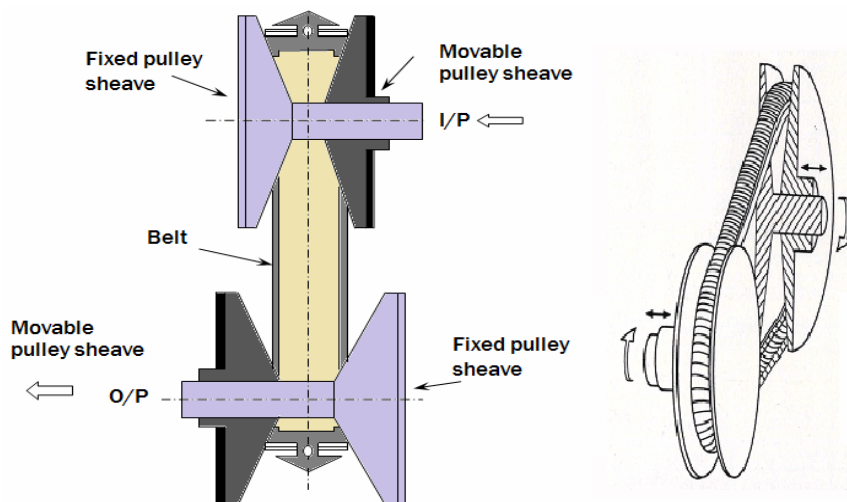


Figure 1: Pulley arrangement

The bands-segment interaction and the inertial effects of the belt were not modeled in detail. Non-dimensional equations were defined to encompass different loading scenarios. [7] Investigated elastic creep velocity of V-belt analytically and experimentally. The belt creep velocity depends not only on the structural characteristics of the belt, but also on the operational characteristics of the CVT. It was observed that the belt creep velocity was a function of transmitted power. The belt dynamics was modeled using quasi-static equilibrium concepts. [8] Investigated the torque transmitting capacity of a metal pushing V-

belt CVT under no load condition on the driven pulley. Their research focused on the microslip behavior of the V-belt due to the redistribution of elemental gaps in the belt. [9, 10] Developed a detailed dynamic model to understand the transient behavior and torque transmitting capacity of a metal V-belt CVT. The inertial coupling due to the radial and tangential motions of the belt was modeled in detail. Flexural effects were neglected and the contact between the belt and the pulley was modeled using continuous Coulomb friction theory. Their work illustrated the importance of belt inertial effects on the torque transmitting capacity of the metal V-belt CVT. They also emphasized on the significance of providing a feasible set of initial operating conditions to the CVT model in order to initiate torque transmission.

2. STEADY STATE MODEL OF A METAL V-BELT CVT

2.3 KINETICS OF PUSH BELT CVT

The CVT system runs at a steady state condition i.e. constant transmission ratio. The driver and driven pulleys run at constant angular velocities and are subjected to loading conditions of torques and axial forces. The belt inertial effects have been neglected, except for the terms arising from the centripetal acceleration of the belt. Figure 2 shows the geometry of the one part of the belt and pulley moves, the tangential slip is modelled on the basis of gap redistribution between the belt elements [11, 12]. Simple geometry gives an expression for the length of the belt as:

$$L = \sqrt{4C^2 - (d_{sec} - d_{pri})^2} + \frac{1}{2}(d_{pri}\beta_{pri} + d_{sec}\beta_{sec}), \quad (1)$$

Since the length of the belt L is known as is the distance between pulley centres C the equation above can be implemented in an iterative program to find corresponding values of primary and second pulley diameters R_{pri} and R_{sec} and β_{pri} and β_{sec} for any value of belt ratio i_{cvt} , in this work the belt ratio is defined in geometric terms, as output radius over input radius, as:

$$i_{cvt} = \frac{R_{sec}}{R_{pri}} = \text{Transmission ratio}, \quad (2)$$

$$\beta_{pri} = \pi - 2 \sin^{-1} \left(\frac{d_{sec} - d_{pri}}{2C} \right) = \pi - 2 \sin^{-1} \left[0.5 \frac{d_{sec}}{C} (1 - i_{cvt}) \right], \quad (3)$$

$$\beta_{pri} = \pi - 2 \sin^{-1} \left(\frac{d_{sec} - d_{pri}}{2C} \right) = \pi - 2 \sin^{-1} \left[0.5 \frac{d_{sec}}{C} (1 - i_{cvt}) \right],$$

$$\beta_{sec} = \pi + 2 \sin^{-1} \left(\frac{d_{sec} - d_{pri}}{2C} \right) = \pi + 2 \sin^{-1} \left[0.5 \frac{d_{sec}}{C} (1 - i_{cvt}) \right], \quad (4)$$

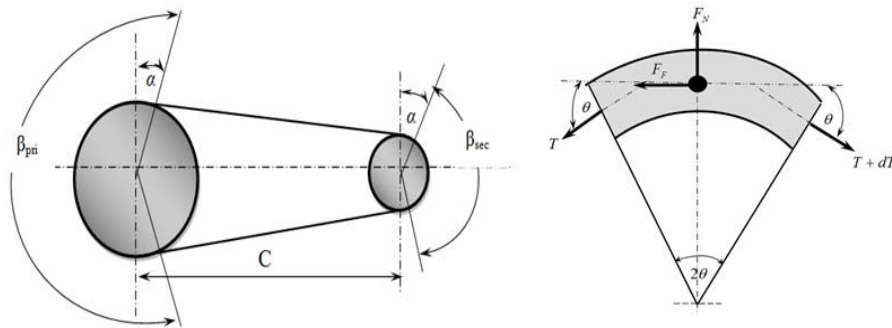


Figure 2 Geometry of the push belt

Figure 3 shows the force acting on the band pack around of belt segments while travelling around a pulley wrap angle:

$$\sum F = 0 \quad \text{in } X \text{ direction}$$

$$(T + dT) \cos \theta = F_F + T \cos \theta, \tag{5}$$

$$T \cos \theta + dT \cos \theta = F_F + T \cos \theta .$$

Since θ is very small, $\cos\theta=1$ and $\sin\theta=\theta$, which may be simplified to:

$$F_F = dT \cos \theta . \tag{6}$$

$$\sum F = 0, \text{ in } Y\text{-direction}$$

$$(T + dT) \sin \theta + T \sin \theta = F_N, \tag{7}$$

$$F_N = (2T + dT) \sin \theta$$

$$\sum F = 0, \text{ -in tangential-direction}$$

$$F_T + F_P \cos \theta = (F_P + dF_P) \cos \theta + F_F .$$

Which may be simplified to:

$$F_T = dF_P \cos \theta + F_F, \tag{8}$$

$$\sum F = 0, \text{ in radial-direction}$$

$$F_N + 2F_R \cos \alpha = F_C + (2F_P + dF_P) \sin \theta + 2N \sin \alpha, \tag{9}$$

Where: $F_C = m \frac{v^2}{R}$

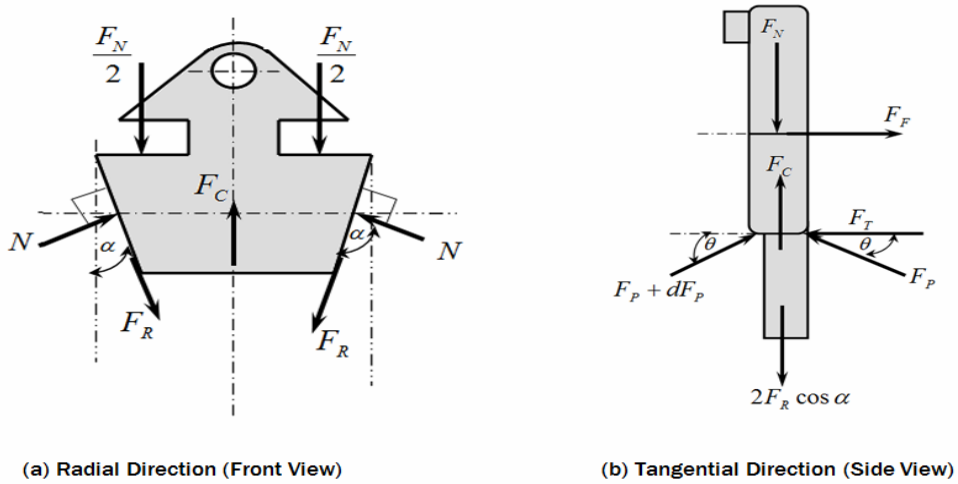


Figure 3: Free body diagram of one segment

2. 4 BELT FRICTION CHARACTERISTICS

The V-belt type CVT utilizes friction to transmit power from the primary pulley to the secondary pulley. The traction curve is the dimensionless relationship between transmitted torque and the slip. The maximum input torque that can be transmitted by the CVT is dependent on the applied clamping force. The belt slip speed and the belt friction coefficient increase when the transmission torque increase. The traction coefficient is therefore chosen to be a dimensionless value [15]. The traction coefficient of primary and secondary side μ_p, μ_s are defined as:

$$\mu_p = \frac{T_p \cos \alpha}{2 F_p R_p} \quad \text{and} \quad \mu_s = \frac{T_s \cos \alpha}{2 F_s R_s}, \tag{10}$$

In which T_p, T_s represent the input and output torque, R_p, R_s represent the primary and secondary running radius of the belt on the pulley, F_p, F_s represent the primary and secondary clamping forces and α is the pulley wedge angle.

The transmission efficiency of the CVT is:

$$\eta_T = \frac{P_{out}}{P_{inp}} = \frac{\omega_s T_s}{\omega_p T_p}. \tag{11}$$

Power loss of the CVT from this equipment is:

$$P_{loss} = P_{inp} - P_{out} = \frac{2 \pi (n_p T_p - n_s T_s)}{60000}, \tag{12}$$

The power loss given by (12) includes slipping losses arising between each contacting component in the CVT, the belt torque loss caused by the resistance to radial resistance and the loss from four bearings supporting the pulley shafts.

3. EXPERIMENTAL WORK

3.1 TEST STAND SETUP

Figure 4 shows the test stand setup for measuring performance of the push belt CVT considered. The experimental work consists of a 18.387 kW (25 Hp), 3000 min⁻¹ induction motor drawing power and driving a CVT belt system of Mitsubishi lancer GLX vehicle gearbox, a separate hydraulic brake that is couple to the output shaft of the CVT. The schematic diagram of the experimental set up with instrumentation details is shown in Figure 5. The motor, hydraulic disc brake, CVT gearbox and hydraulic shift system are hard mounted and aligned on a bedplate. The bedplate is mounted using isolation feet to prevent vibration transmission to the floor. The shafts are connected with both flexible and rigid couplings.



Figure 4: Photograph of the test rig layout

3.2 HYDRAULIC CIRCUIT AND MEASURING

The measurement methodology used induction (1.103 kW, 1450 min⁻¹) motor drawing power through a electrical source and driving hydraulic pump, the hydraulic shift system characteristics are as follows in table 1. The hydraulic part of the CVT essentially consists of a gear pump directly connected to the driving electrical motor, the Directional Control Valve (DCV), choke valves and a pressure cylinder of the moveable pulley sheaves. The volume between the pump and the chock valves including the secondary pulley cylinder is referred to as the secondary circuit, the volume directly connected to and plus the primary pulley cylinder is the primary circuit. Excessive flow in the secondary circuit bleeds off towards the accessories, whereas the primary circuit can blow off towards the drain. Pressures are defined relative to the atmospheric drain pressure pT. The Directional Control Valve (DCV) directs the pressurized fluid to either primary or secondary pulley as set to position A or B. In neutral position the DCV returns the fluid to the tank. The Choke Valves (CV), the throttle choke valve allows the pressure flow normally in the forward direction, and restricts (choke) the flow in the return direction. It is used here to maintain the pressure level in the pulley after shifting the pressure direction to the other pulley, the connection and operation of hydraulic shift system shows in Fig. 6. As the model will only be used to determine the hydraulic system constraints needed for the feed forward control, the following assumptions have been made:

- The compressibility of the oil is neglected
- The oil temperature is constant and all leakage flows are negligible.

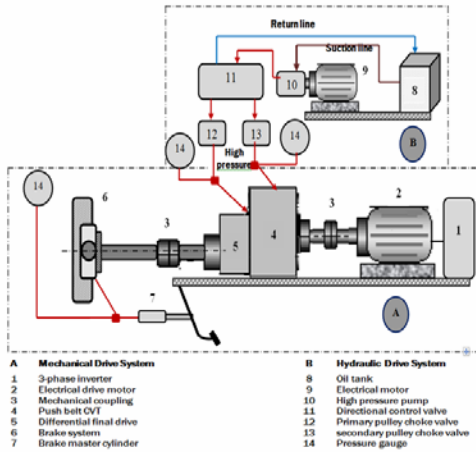


Figure 5: Test stand layout

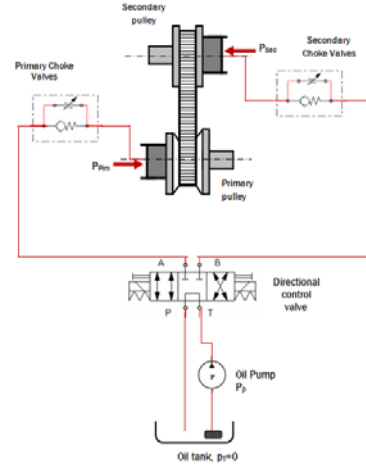


Figure 6: Schematic diagram of hydraulic control circuit

The clamping forces F_p and F_s are realized mainly by the hydraulic cylinders on the moveable sheaves. Since the cylinders are an integral part of the pulleys, they rotate with an often very high speed, so centrifugal effects have to be taken into account and the pressure in the cylinders will not be homogeneous. Therefore, the clamping forces will also depend on the pulley speeds ω_{pri} and ω_{sec} . Furthermore, a prestressed linear elastic spring with stiffness K_s is attached to the moveable secondary sheave. This spring has to guarantee a minimal clamping force when the hydraulic system fails. Together this results in the following relations for the clamping forces:

$$F_p = P_p * A_p + C_p * \omega_{pri}^2 \quad (13)$$

Here, A_p is the primary piston area, C_p a centrifugal coefficient and P_p the oil pressure in the primary circuit.

$$F_s = P_s * A_s + C_s * \omega_{sec}^2 + K_s \Delta x + F_i \quad (14)$$

Likewise, the secondary pulley clamping force F_s consists of a direct pressure term $P_s * A_s$ and a centrifugal force, with A_s the secondary piston surface, C_s the centrifugal coefficient and P_s the secondary pressure. Moreover, in F_s there is a contribution of the secondary spring F_{spr} that has to warrant a minimal clamping force under all circumstances. F_i is the force in the spring if the secondary moveable sheave is at position $\Delta x = 0$. The oil flow from the (DCV) to the primary circuit, by use the law of mass conservation, applied to the primary circuit:

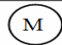
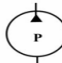
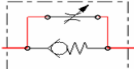
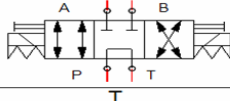

$$Q_{DCV \rightarrow p} = C_f * A_p * x_p \sqrt{\frac{2(p_s - p_p)}{\rho} \text{sign}(p_s - p_p)}, \quad (15)$$

where C_f is a constant flow coefficient and ρ is the oil density. The equivalent valve opening area A_{sp} depends on the primary valve stem position x_p . The oil flow from the primary circuit to the drain

$$Q_{p \rightarrow d} = C_f * A_{pd} * x_p \sqrt{\frac{2(p_p)}{\rho}}, \tag{16}$$

A_{pd} is the equivalent opening area of the primary valve for the flow from primary circuit to the drain.

Table 1: Hydraulic system characteristics

No.	Component	Specification	Values	Symbol
1	Drive Motor	Power Voltage Current	1.5 HP 1420 rpm 220/230 V 9.82 Amp	
2	Hydraulic Pump	Flow rate Max. pressure	10Liter/min 10 bar @ 1420 rpm	
3	Choke Valves	Flow rate	15 litre/ min	
4	Directional control valve	Flow rate Operated Position Ports Center	30 liter/min Mechanically Operated 3position 4ports Closed Center	
5	Oil Tank	Capacity	Up to 15 liter Capacity	

The oil flow from the (DCV) to the secondary circuit, by use the law of mass conservation, applied to the secondary circuit

$$Q_{DCV \rightarrow S} = C_f * A_s * x_s \sqrt{\frac{2(p_p - p_s)}{\rho}} \text{sign}(p_p - p_s), \tag{17}$$

Application of the law of mass conservation to the hydraulic circuit yields, the flow rate of oil pump is written as:

$$Q_{pump} = Q_{DCV \rightarrow S} + Q_{DCV \rightarrow p} + Q_{p \rightarrow d}, \tag{18}$$

Root mean square is a kind of average of pressure and clamping force signal, for discrete signals, the RMS value is defined as:

$$RMS = \sqrt{\frac{1}{N} \sum_{n=1}^N (x(n) - \bar{x})^2}, \tag{19}$$

$$\bar{x} = \frac{1}{N} \sum_{n=1}^N x(n).$$

where N is the number of samples taken within the signal and $x(n)$ the time domain signal and \bar{x} is the mean value of all the amplitudes.

4. RESULTS AND DISCUSSIONS

4.1 MODELLING RESULTS

The simulations were conducted on MATLAB platform. The model required the input of design or configuration parameters. The characteristics of the metal belt CVT that influence its response to the loading conditions numerous simulations were done for different loading conditions in order to understand the dynamics of CVT under steady-state conditions. The impending motion in the model is such that the belt starts to move downwards in the driver pulley sheave and upwards in the driven pulley sheave. The transmission ratio for the model is defined as the ratio of belt pitch radius on driver pulley to

belt pitch radius on driven pulley. Table 2 gives some of the parameter values used for simulation:

Figure 7 and Figure 8 show the calculated pulley radii and angles of wrap about each pulley respectively for the complete range of ratios. Using the ratio definition described above a ‘high ratio’ or ‘overdrive’ condition is described by a ratio value i_{cvt} of less than one.

Table 2 Main parameters of CVT model data

No.	Parameters	Symbols	Units	Values
1	Coefficient of friction	μ	–	0.15
2	Centre distance	C	m	0.245
3	Half Pulley Wedge Angle	θ	Deg.	13
4	Unit belt mass	m	kg/m	0.245
5	number of bands	i_p	–	6
6	Thickness of an individual band	t_{band}	m	$0.218 \cdot 10^{-3}$
7	Thickness of one segment	t_{sag}	m	$5.58 \cdot 10^{-3}$
8	Max. input torque	T_i	N.m	400

The simulation result with constant value of input speed 1600 rpm and torque 120 N.m as illustrate in Figures 9 and Figures 10, in Figure 9 show the tensile force profiles for the band pack on the driver and driven pulleys. The band tensile force decreases from the inlet to the exit of the driver pulley, whereas, it increases from the inlet to the exit of the driven pulley. The elements pack up as the belt moves around the pulleys, and consequently the compressive force in the belt increases. Figure 10 shows the compressive force profiles on both the driver and the driven sides. It is noted from the figure that there exists a region over the pulley wrap where the compressive force does not build up; this is the inactive arc region.

Figure 11 illustrates the transmission torque with transmission ratio at different values of clamping force 1000 and 6000N at high value of axial force or clamping force to result the increase the transmission torque. Also highlights that the model is able to sustain lower load torque conditions at higher transmission ratios than at lower transmission ratios. Figure 12 shows the modelling results of the effective traction coefficient with different reduction ratios.

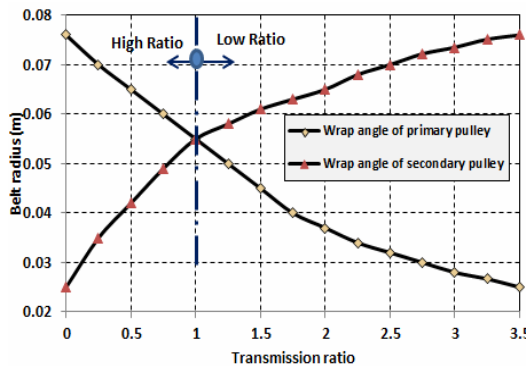


Figure 7 Belt Radii vs with transmission ratio

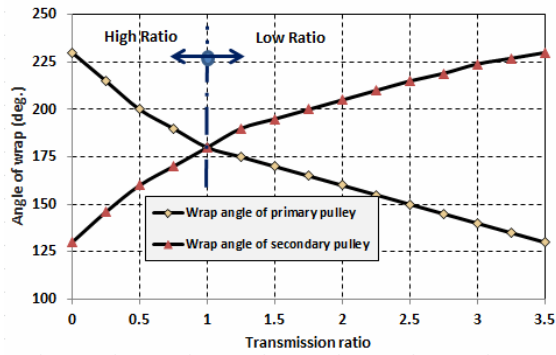


Figure 8 Variator Wrap Angles vs transmission ratio

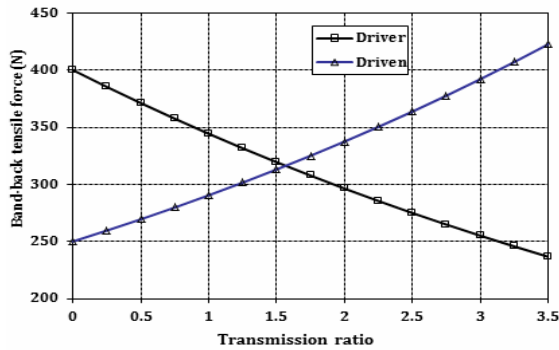


Figure 9 Band pack tensile force on the driver and driven pulleys

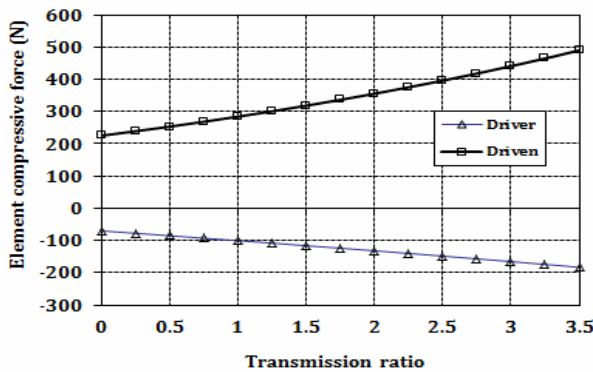


Figure 10 Belt element compressive force on the driver and driven pulleys

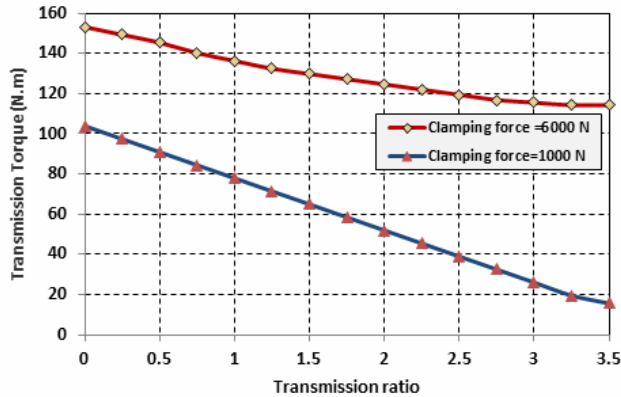


Figure 11 Transmission torque with transmission ratio vs with transmission ratio

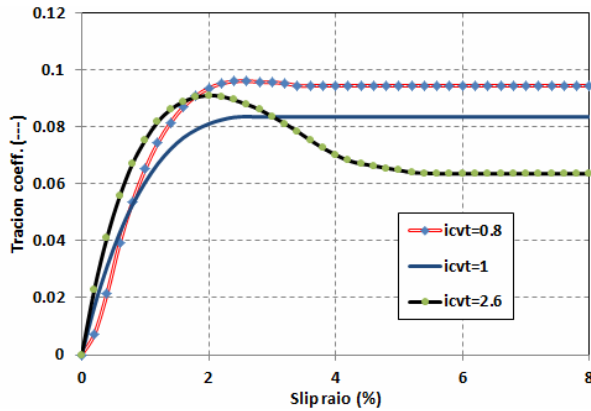


Figure 12 Traction coefficient vs slip ratio at different reduction ratios

4. 2 PRACTICAL RESULTS

This section will present the results obtained from the tests carried on the push belt CVT system in the laboratory. The results will be discussed to determining the performance and response of push belt include different oil pressure and transmission ratio. A National Instruments LabVIEW™ program version 7.1 was used to create the desire software program to perform the tests required. The speed variation can be accomplished by varying the frequency to the motor with a AC inverter unit. The motor shaft speed from 800 rpm to 2400 rpm; and the load variation values by hydraulic brake system from zero to 75 N.m.

Figure 13 and figure 14 show the samples from the translation primary and secondary pressure responses in terms of time-domain, with different input speed 800 and 2400 rpm. Figure 15 and figure 16 show the samples from the translation primary and secondary clamping responses in terms of time-domain. The other results show in the section comparison of result. The maximum oil pressure acting on secondary pulley piston is 48 bars at input speed 800 rpm and decrease to 45 bars at increased the input speed to 2400 rpm.

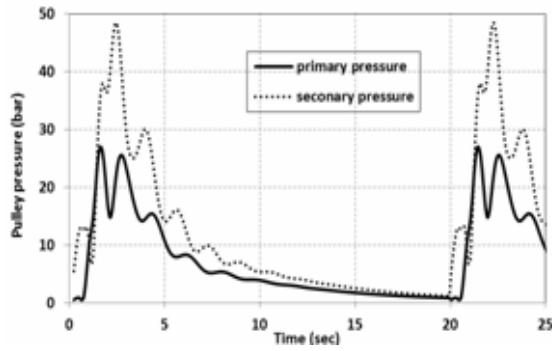


Figure 13 Translation primary and secondary pressure responses at $\omega_p=800rpm$

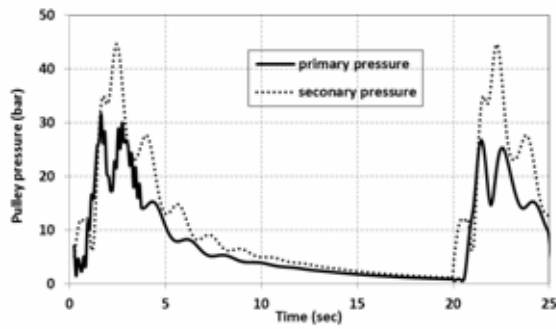


Figure 14 Translation primary and secondary pressure

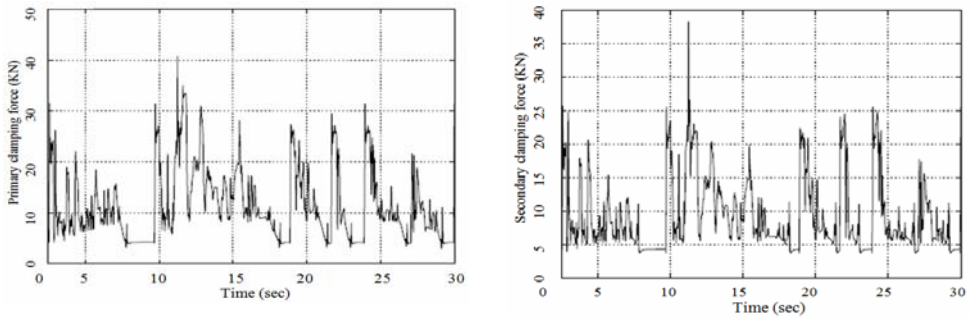


Figure 15 The primary and secondary clamping force responses at $\omega_p=800rpm$

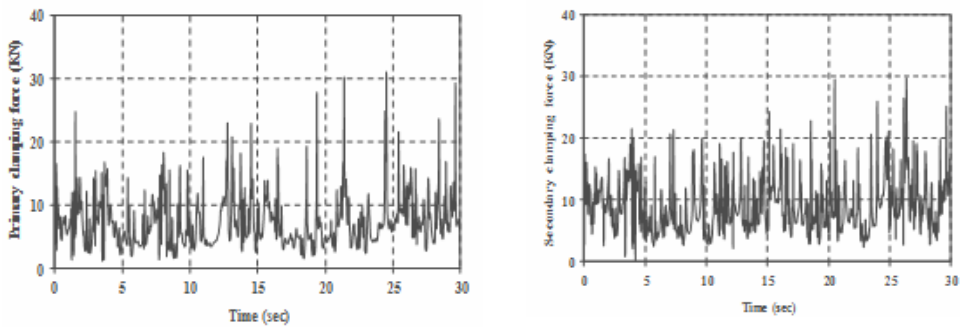


Figure 16 The primary and secondary clamping force responses at $\omega_p = 2400\text{rpm}$

4.3 COMPARISON OF SYSTEM RESULTS

The comparison between theoretical and experimental results at 1600 rpm show in figures 17 and 18 in figure 17 shows the traction coefficient at different transmission ratio, the measured clamping force effect on the fluctuations of the traction coefficient. Figure 18 illustrates the transmission efficiency at $i=2.6$, the maximum value of efficiency equal 94% at theoretical and $90 \pm 2\%$ at experimental, the efficiency depends on oil pressure, transmission ratio and input speed. Figures 19 and 20 illustrate the RMS of clamping force with different output load and different speed and $i=2.6$. Figure 21 illustrates the maximum value of transmission efficiency with different clamping force. The transmission efficient of the CVT increases with decreasing clamping force and the transmission ratio are kept constant.

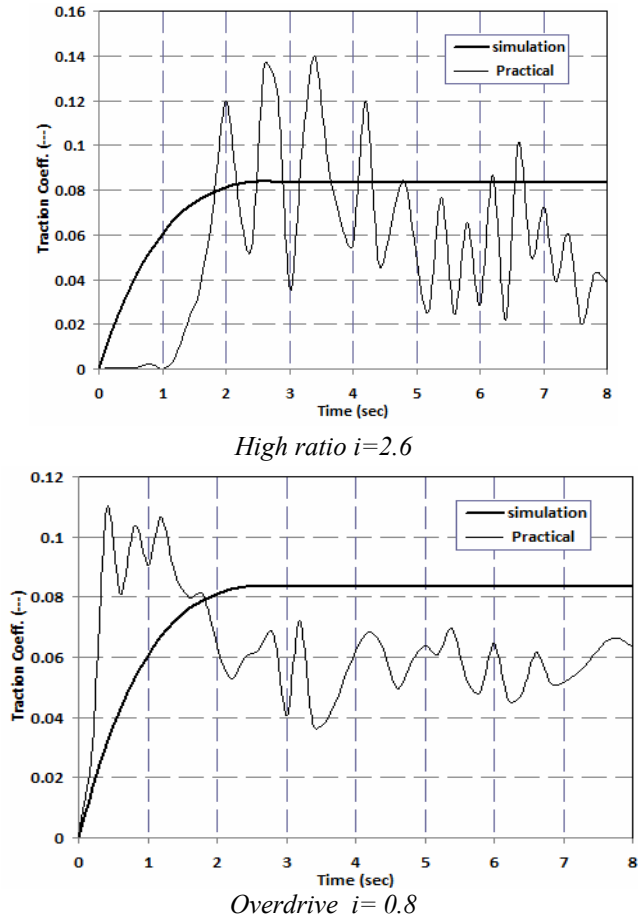


Figure 17 Comparison between simulation and practical traction coefficient = 1600rpm

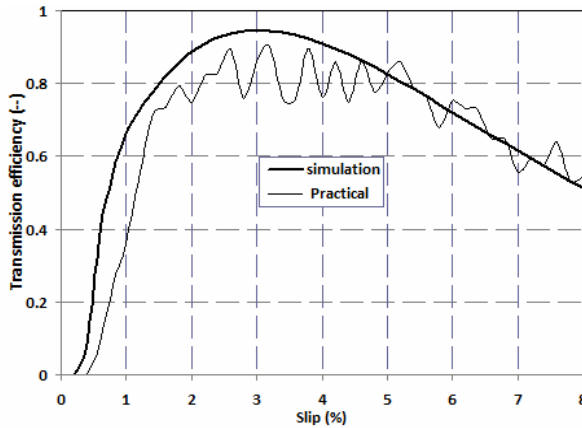


Figure 18 Comparison between simulation and practical of transmission efficiency =1600rpm

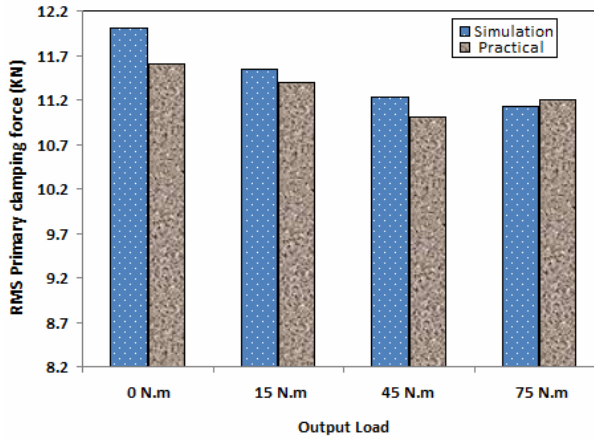


Figure 19 Comparison between simulation and practical of clamping force RMS =1600rpm

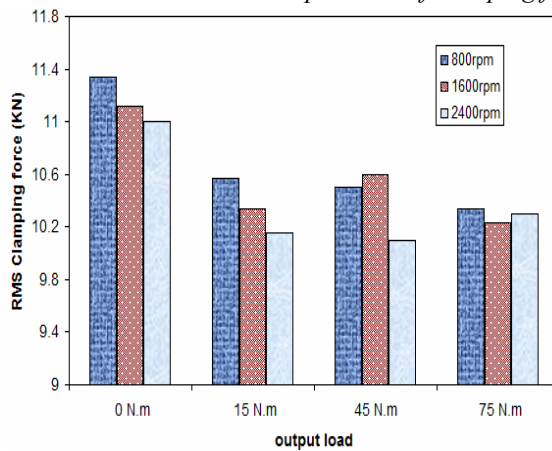


Figure 20 RMS of practical clamping force with different input speed

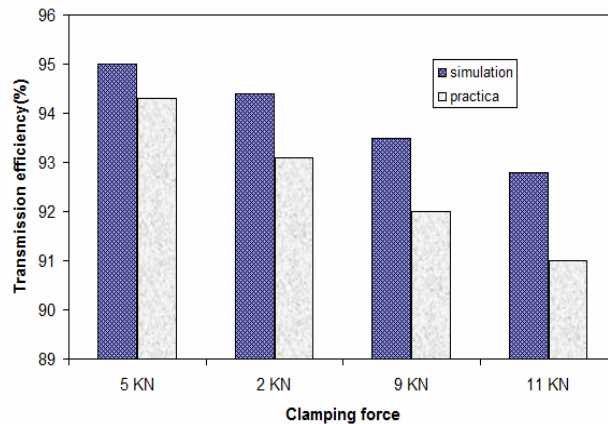


Figure 21 Comparison between simulation and practical of maximum transmission efficiency with different clamping force

5. CONCLUSIONS AND RECOMMENDATIONS

In this paper, we present the dynamic analysis and experimental evaluation of a one type of CVT. The main conclusions from the work carried out summarized in the following points:

Applying the different input variable parameters to the bush belt full system mathematical model which are the input speed (ω_p), the transmission ratio (i_{cvt}), the half pulley wedge angle (θ), and the slip ratio, that directly affects the system transmission performance.

Based on the RMS of applied pressure and clamping force of CVT gearbox, the influence of changing gearbox speed and load on the RMS value is also introduced, which confirm the discussion stated above.

The laboratory apparatus and experimental methodology capability established in this work could be utilized for evaluating the dynamic performance of the push belt CVT.

The investigated the reliability of the improved model with a theoretical-experimental comparison of a belt drive variator in steady state conditions. Our calculations have shown a good agreement between theory and experiments especially at high clamping forces values, either in predicting the thrust force ratio necessary to establish the desired transmission ratio either in evaluating the variator traction behaviour.

6. REFERENCES

- [1] Lingyuan Kong, Robert G. Parker “Steady mechanics of layered, multi-band belt drive used in continuously variable transmissions (CVT)”science direct Mechanism and Machine Theory 43 (2008) 171–185.
- [2] Shinya K., Toru Fujii, Shigera K. “Study on a Metal pushing V-belt Type CVT: Band Tension and Load Distribution in Steel rings” ELSEVIER, March 1999, JSAE 20(1999)55-60.
- [3] Shafie A., Ali M. H. “Development of an Efficient CVT using Electromechanically System” World Academy of Science, Engineering and Technology 56, 2009.

- [4] Mohan Gangadurl, Harikrishnan B., Sreekumar H. "Development of an Analytical Design Concept of Mechanical Controlled continuously Variable Transmission" SAE, 2005-26-069.
- [5] Bonsen B., Klaassen T.W.G.L., K.G.O. van de Meerakker" Modeling Slip- and Creep-mode Shift Speed Characteristics of a Push-belt Type Continuously Variable Transmission" 04CVT-3
- [6] Allen, Mark and LeMaster, Robert. "A Hybrid Transmission for SAE Mini Baja Vehicles". SAE Publication 2003-32-0045.
- [7] Micklem J. D., Longmore D. K., Burrows C. R., "Modeling of the Steel Pushing V-belt Continuously Variable Transmission", Proceedings Inst. Mech. Engineers Vol. 208 Part C: pp. 13-27.
- [8] Shimizu H., Kobayashi D., Kawashima J., Kato Y., "Development of 3-D Simulation for Analyzing the Dynamic Behavior of a Metal Pushing V-Belt for CVTs", SAE Paper, 2000-01-0828, SAE special publication (SP-1522), transmission and driveline symposium 2000, pp. 31-36.
- [9] Kurosawa M., Kobayashi M. and Tominaga M. "Development of a High Torque Capacity Belt Drive CVT with a Torque Converter" ELSEVIER, July 1998, JSAE 20(1999)281-287.
- [10] Pennings B., Mark van D., Arjen B., Erik van G. and Marlène L. "Van Doorne CVT Fluid Test: A Test Method on Belt-Pulley Level to Select Fluids for Push Belt CVT. Applications" 2003 SAE International P.N 2003-01-3253.
- [11] Christopher R. W. "A Kinematic Analysis and Design of a Continuously Variable Transmission" Master of Science in Mechanical Engineering, 19 January 2006.
- [12] Zhijian Lu "Acceleration Simulation of a Vehicle with a Continuously Variable Power Split Transmission" Master of Science in Mechanical Engineering, July 29, 1998

¹ACTIVE NUMERICAL VEHICLE ACCELERATION CONTROL ALONG ACCELERATION FUNCTION WITH MAXIMUM ENGINE TORQUE EFFICIENCY

Ivan Dunderski

UDC: 629.331.5; 62.529:559

Summary

The paper explores ways to increase effectiveness of vehicle acceleration. New solution has been given, based on the numerical control of engine torque using acceleration function.

Natural engine torque is replaced by a curve of maximum efficiency of the engine torque, which passes through the torque maximums of partial engine charges.

To control vehicle acceleration by the acceleration function torque controller is designed and connected to the engine electronic control unit (ECU). Programming code is written for controller operation. The study, that was conducted on an experimental vehicle, confirmed the feasibility of the numerical control of vehicle acceleration by the acceleration function with maximum torque effectiveness. Principal objective of this paper is how to improve engine torque effectiveness while vehicle accelerates in order to save fuel. The scope of investigation is replacing natural engine torque curve by a curve of maximal efficiency of the engine torque. Methodology employed in this paper is physical – mathematical model, computer simulation and processing, controller programming and experimentation. Vehicle acceleration employs custom designed controller by the acceleration function torque controller. Programming code is written for controller numerical operation. Experimental results and principal conclusions are that the control of vehicle acceleration by acceleration function saves fuel

Key words: Controlled vehicle acceleration, the function of acceleration, engine torque efficiency

AKTIVNO UPRAVLJANJE UBRZANJEM VOZILA NUMERIČKOM KONTROLOM PO FUNKCIJI UBRZANJA SA MAKSIMALNOM EFEKTIVNOŠĆU MOMENTA MOTORA

UDC 629.331.5; 62.529: 559

Rad istražuje načine za povećanje efektivnost ubrzanja vozila. Dato je novo rešenje, zasnovano na numeričkom upravljanja obrtnog momenta motora po funkciji ubrzanja. Prirodna kriva momenta motora zamenjena je krivom maksimalne efektivnosti momenta motora, koja prolazi kroz maksimume momenata delimičnih punjenja motora. Za upravljanje ubrzanjem vozila po funkciji ubrzanja napravljen je kontroler obrtnog momenta

¹ *Received: February 2013, Revised May 2013, Accepted July 2013.*

i povezan sa elektronskom upravljačkom jedinicom motora. Napisan je programski kod za rad kontrolera. Istraživanje sprovedeno na eksperimentalnom vozilu potvrdilo je ostvarivost numeričkog upravljanja ubrzanjem vozila po funkciji ubrzanja sa maksimalnom efektivnošću momenta motora.

Ključne reči: Upravljanje ubrzanje vozila, funkcija ubrzanja, efektivnost momenta motora

ACTIVE NUMERICAL VEHICLE ACCELERATION CONTROL ALONG ACCELERATION FUNCTION WITH MAXIMUM ENGINE TORQUE EFFICIENCY

Ivan Dunderski¹, M.Sc. ME, Lecturer

UDC: 629.331.5; 62.529: 559

1. INTRODUCTION

Vehicle and engine development is a continuous process which focuses on improvement of vehicle dynamic characteristics, increase of engine torque and power and reduction of energy requirements for vehicle motion. Increase of performance and reduction of energy consumption are opposite requirements resulting in modern vehicles being equipped with mechatronic systems that control vehicle motion dynamics, engine and transmission operation.

Special attention is directed toward control of amount and composition of the exhaust gases produced in the combustion process in the engine and its impact on the environment. Operation of Otto and diesel engine is regulated by electronic control unit (ECU), which optimizes fuel consumption and exhaust gas composition. In an ideal (stoichiometric) combustion of the mixture, the products of a chemical reaction are carbon dioxide (CO₂) and water (H₂O).

Carbon dioxide is a non-toxic gas, found in mixture of gases [1,2], which creates the greenhouse effect. The only way to reduce the amount of CO₂ in the exhaust gases produced by hydrocarbon fuels combustion is to reduce fuel consumption.

During mixture combustion in the engine, additional inevitable chemical reaction products occur, which are carbon monoxide (CO), unburnt hydrocarbons (HC) and nitrogen oxides (NO_x) in Otto engine and particles of carbon (C) in diesel engine. These substances are toxic. Their conversion into non-toxic substances is carried out catalytic converter and particle filter.

On the other hand, the fuel consumption is greatly influenced by vehicle motion. Vehicle motion depends on driver's skill and desire to adapt their driving to traffic and road conditions. The vehicle generally moves with variable velocity.

While moving vehicle at a constant speed, $v=const$, minimal energy must be invested to overcome the resistance movement. Inertial resistance, related to the acceleration does not exist, because the $dv/dt=0$.

While moving vehicle that accelerates, fuel consumption is very dependent on the magnitude of acceleration a and rate of change of acceleration $\dot{a}=da/dt$. Inertial resistance is present. All members in the power balance equation, except air resistance, include mass, which acceleration may take up to 40% of total fuel consumption, during city ride [2].

Inertial resistance features acceleration and masses that both rotate and translate.

In order to save fuel, it's necessary to control the way vehicle accelerates and to reduce vehicle, engine and transmission mass.

¹ Ivan Dunderski, MSc, ME, lecturer, School of Electrical Engineering and Computer Science Applied Studies, University of Belgrade, ivand@viser.edu.rs

Mass reduction is issue of design, but vehicle acceleration control must be achieved in the interaction with the driver. The technical part of interaction incorporates two components:

- Reduction of engine torque
- Delay in throttle response

The magnitude of acceleration $a=dv/dt$ is controlled, by reducing engine torque. Engine speed, torque and throttle functional relations are redefined and remapped. Engine computer is reprogrammed. This saves fuel because the less torque requires less fuel per engine cycle. Disadvantage: Loss of dynamical characteristics of vehicle.

Delay in throttle response controls the rate of change of acceleration $\dot{a}=da/dt$. Throttle to accelerator pedal functional relation is redefined and electronic accelerator pedal is reprogrammed.

Avoiding rapid acceleration changes saves fuel, because they require additional amount of fuel and rich mixture, $\lambda < 1$, in order to speed up combustion. Exhaust gas composition is worsened.

Disadvantage: Loss of drivability

Torques are reduced via driving modes [3].

Figure 1 shows driving modes for vehicle „Subaru Impreza“, made by vehicle manufacturer in Japan: „Intelligent“, „Sport“ i „Sport Sharp“.

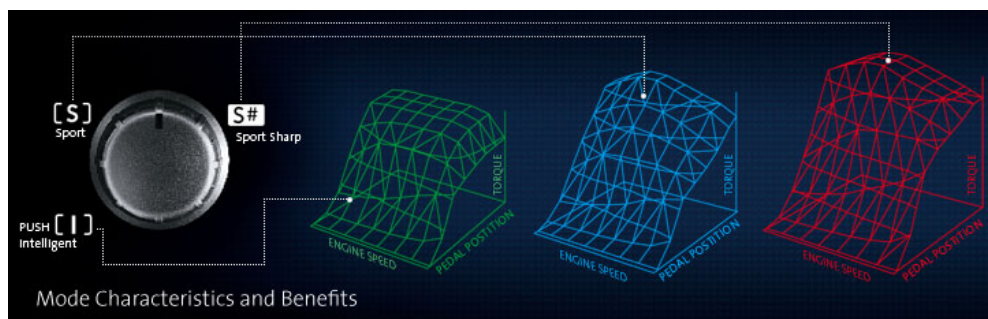


Figure 1: Driving mode selection [3]

Engine torque to accelerator pedal and engine speed mapping

Mode „Sport Sharp“, „S#“ is source engine operating mode. Mode „Sport“, „S“, is very similar to source mode in terms of mapping shape, but torques for same accelerator pedal position are reduced. Mode „Intelligent“, „I“ continues with further torque reduction, in addition with surface flattening in area of maximum engine torques.

Comparison of engine torques in relation to driving modes is shown in Figure 2.

Engine is turbo-charged, which allows constant torque over wide range of engine speed.

The maximum torque T reduction is the greatest while using the most conservative mode „Intelligent“. Consequently, loss of power $P=T\omega$ as a product of torque T and engine speed ω , is also the greatest.

„Intelligent“ mode is suitable for city ride, where vehicle speeds v are low and the road is mostly horizontal. Acceleration a and its rate of change da/dt may be small. The need for power P for overcoming drag resistance R_{drag} is low, since vehicle speeds are also low.

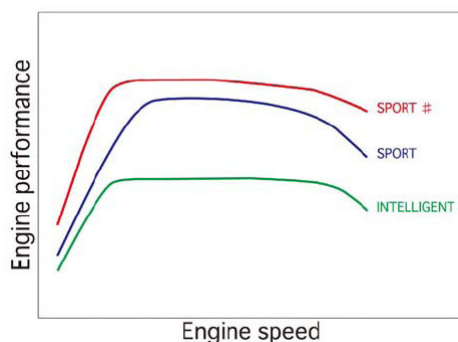


Figure 2: Engine torques for „Intelligent“, „Sport“ i „Sport Sharp“ driving modes [4]
Accelerator pedal response is slowed by reprogramming Electronic Throttle Control (ETC).

Figure 3. illustrates accelerator pedal response to pressure. In all three modes the accelerator pedal is fully pressed (100%).

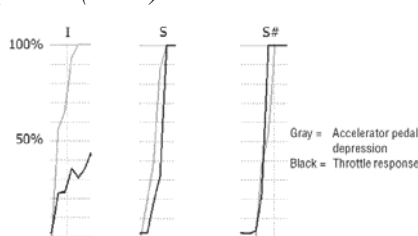


Figure 3: Accelerator pedal response [5]

Accelerator pedal response delay in „I“ mode is large and nonlinear, while delay in „S“ mode is small and linear. In „S#“ mode, response is linear and ETC catches up with accelerator pedal pressure around 40% of its full movement. Further ETC response goes even before current pedal pressure: Drivability is additionally increased. Similar idea is used for braking pedal, when driver receives aid in rapid boost of maximum pressure in braking installations. The Bosch company is continuously upgrading this system.

Other vehicle manufacturers around the world are following the same idea for fuel saving. Names for the individual driving modes are different. Mode which corresponds to the "Intelligent" mode is usually called "ECO/Economic", and the original mode is "Standard."

Driver's impact on fuel consumption is significant. The vehicle manufacturer "Ford Focus" from the United States (European branch) states that interaction with the driver alone can result in fuel savings of up to 24%. [6].

The vehicle does not have technical solutions in terms of reprogramming torque maps and response to the accelerator pedal delays. Instead, a pure software solution is applied to monitor and collect ride data. It records the engine speed, vehicle speed, and accelerator pedal position, the position of the clutch pedal, selected gear and engine operating temperature. The collected data are analyzed and processed.

The result is evaluation of driving style, which is reported to the driver. Proposal of solution for fuel-saving is in form of guidelines for changes in driving style. Tips are presented on a small display, Figure 4.



Figure 4: Driving style tips display [6]

Criteria for evaluation of driving style are:

Gear: Does driver use the highest gear that traffic conditions permit

Anticipation: Does driver keep his distance from other vehicles so that he does not need to suddenly brake or accelerate

Speed: Is driver using the system that control speed (cruise ctrl.) on the open road

The 1st criteria suggests avoiding usage of an unnecessary power $P=T\omega$. When there is enough torque T , engine speed ω reduction is achieved by shifting to higher transmission ratio, which makes the engine operate at lower speed resulting in decreasing number engine cycles for the same road length, saving fuel.

The 2nd criteria's aim is that vehicle maintains constant speed, $v=const$, as long as it's possible. Unnecessary braking drains kinetic energy and unnecessary acceleration requires additional kinetic energy.

The 3rd criteria is a trade-off for the 2nd ($v=const$). The driver delegates vehicle motion control to the „Cruise Control“ system [7].

To sum up, the influential factors on fuel consumption are:

- Engine operation condition
- Vehicle acceleration way
- Vehicle mass magnitude

This paper defines the engine operation way and vehicle acceleration way in order to reduce fuel consumption. The influence of the mass on the dynamic characteristics of vehicle and ways to reduce masses are presented in the paper [2].

Following guidelines are adopted for control of engine operation during vehicle acceleration:

- Maximization of engine operation efficiency
- Optimization of vehicle acceleration performance
- Exclude drivers influence on engine operation

This paper presents active control of vehicle acceleration by numerical control of engine torque T using acceleration function that gives maximum efficiency of engine operation.

2. APPROACH TO PROBLEM

A speed characteristics of engine torque is defined by engine torque curve family. The „external“ characteristic curve determines torque values in relation to engine speed for maximum engine charge. The „internal“ characteristic curves corresponds to partial engine charge. Engine charge is determined by engine throttle angle $\theta_i(h)$ which corresponds to accelerator pedal position h .

The lesser the engine charge is, the lower the maximum torque and engine speed, for family curve that corresponds to given engine charge. Also, the torque reaches its maximum value at lower engine speed.

The common characteristics curve connects points of maximum of particular family curves, Figure 5.

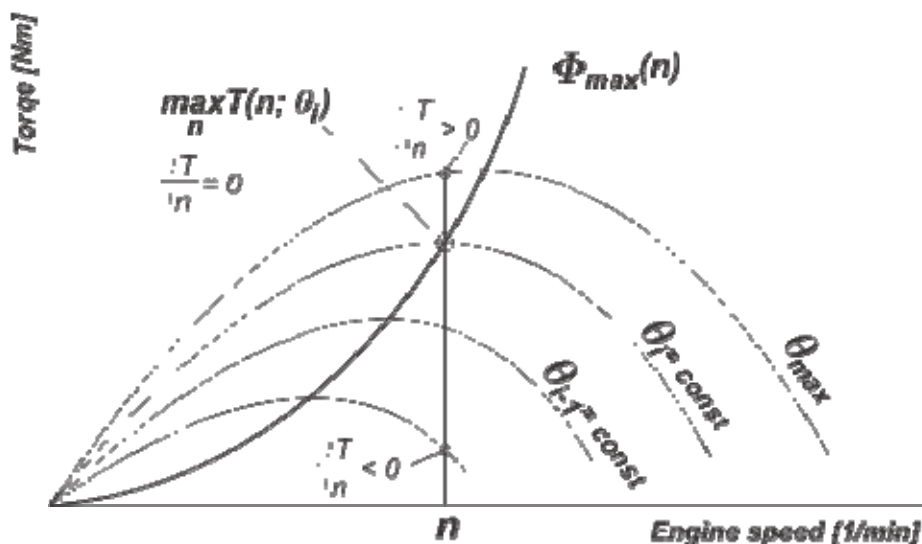


Figure 5: The common characteristic of torque curves family

The common characteristic of torque curves family is given by expression:

$$\Phi_{\max}(n) = \left\{ T(n; \theta_i) \mid \theta_i : \frac{\partial T}{\partial n}(n; \theta_i) = 0 \right\}$$

Torque curves, for natural aspirated engine, have one maximum and inflection points.

2.1 ENGINE TORQUE EFFICIENCY DURING VEHICLE ACCELERATION

For any torque family curve member i , which corresponds to throttle angle θ_i , the torque $T(n; \theta_i)$, depending on engine speed value, is lesser or equal to maximum value of that family member.

Acceleration of the vehicle is always conducted along one of the family curves. During acceleration, going from minimum to maximum engine speed value, the torque increases, reaches a maximum and then decreases. Engine torque efficiency η_T reaches its peak at the maximum torque. Before and after engine speed value n_i that corresponds to the maximum torque value, engine efficiency is lesser than its peak, as lesser torque is developed, Figure 6.

Maximum engine efficiency $\eta_T = \max$ is realized when vehicle accelerates along the common characteristics $\Phi_{\max}(n)$ of torque family, because it passes through maximum torque values for particular engine charge.

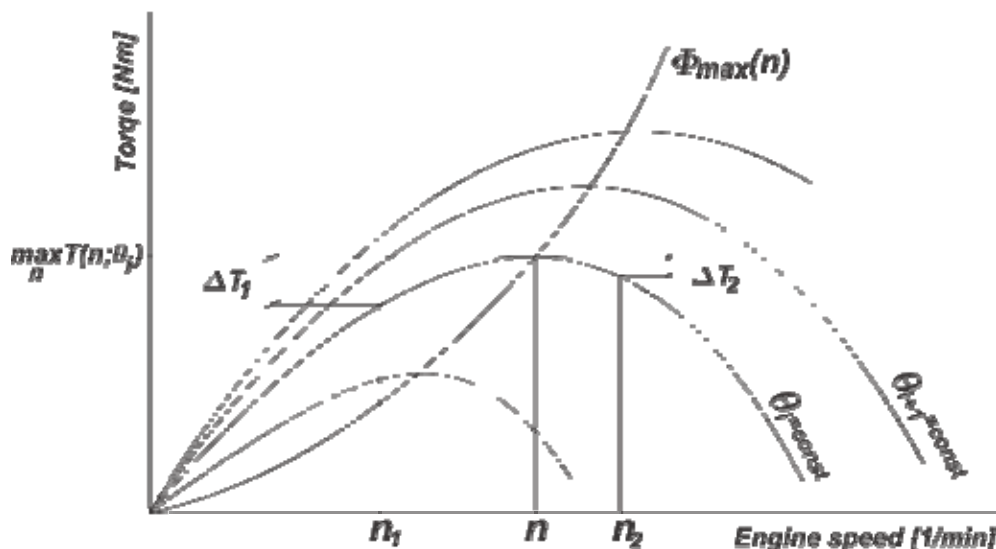


Figure 6: Engine torque efficiency

$$\max_n T(n; \theta_i) = T(n_2; \theta_i) + \Delta T_1 = T(n_2; \theta_i) + \Delta T_2$$

$$\eta_T = \frac{T(n; \theta_i)}{\max_n T(n; \theta_i)} \leq 1$$

Engine speed value n range in which the peak efficiency can be achieved, is defined by common characteristics curve domain:

$$n_{min} \leq n \leq n_T$$

n_{min} – the lowest engine speed value required to move the vehicle

n_T – engine speed value that corresponds to maximum torque for external characteristics

(For contemporary vehicles $n_T \sim 3500$ [min⁻¹].)

Vehicle acceleration controlled by driver is conducted by setting accelerator pedal position h . Once the accelerator pedal position is set, the driver, usually, does not change it during vehicle acceleration, $h = \text{const}$.

Vehicle acceleration along the common characteristic $\Phi_{max}(n)$ requires continuous charge modification, $\theta_i \neq \text{const}$, because common characteristic consists of torque maximums for various engine charges. By operating accelerator pedal, the driver is unable to realize this relation $h \rightarrow \theta_i \rightarrow \Phi_{max}(n)$. To achieve engine charge that follows common characteristic curve, active control system for vehicle acceleration is needed.

For active vehicle acceleration, control is required via electronic system:

- Engine torque controller (hardware)
- Algorithm that accelerates vehicle (software)

Base information set for control are:

- Engine torque curve family, $T(n; \theta_i)$ and

- Common characteristic curve, $\varphi_{\max}(n)$

2. 2 VEHICLE ACCELERATION PERFORMANCE AND ENGINE TORQUE EFFICIENCY

Figure 7 shows comparison of torque values T , T_e , T_R , for fixed engine speed value n .

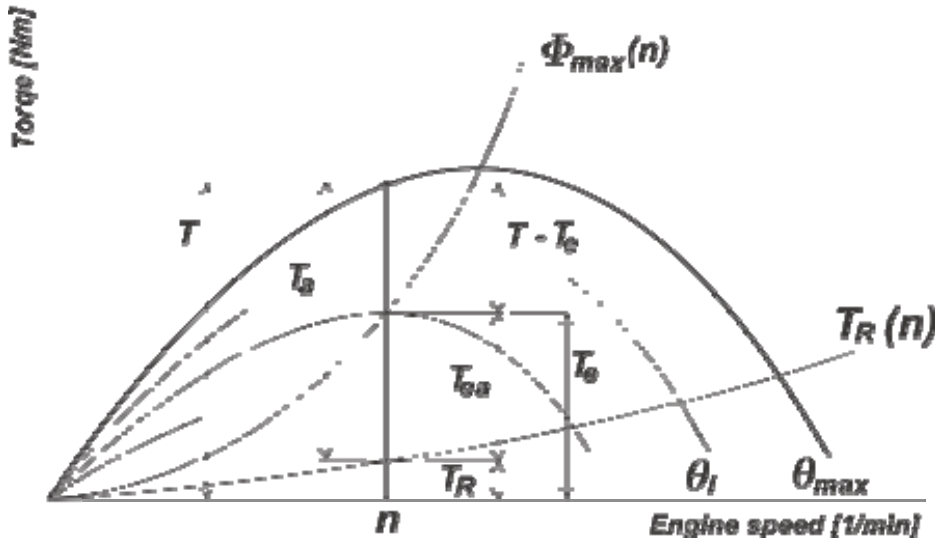


Figure 7: Comparison of engine torques along torque curve family with torques along acceleration function; Vehicle resistance torques

Values given in Figure 7 are:

- T – torque value that corresponds to external characteristics
- T_e – torque value that corresponds to common characteristics $\varphi_{\max}(n)$
- T_R – torque values of road resistance
- T_e – torque on common characteristic for a particular charge
- T_{ea} – torque available for vehicle acceleration

After overcoming road resistance torque T_R , remaining torque T_a for vehicle acceleration along external characteristics is

$$T_a = T - T_R$$

Remaining torque T_{ea} or vehicle acceleration along external characteristics is

$$T_{ea} = T_e - T_R$$

Torque difference ΔT between torque T_a and torque T_{ea} for vehicle acceleration along common characteristics is

$$\Delta T = T - T_e$$

As engine speed n increases, that difference converges to zero: $\Delta T \rightarrow 0$

In other words, with engine speed value n increase, vehicle acceleration performance along common characteristic $\varphi_{\max}(n)$ continuously approach acceleration performance along external characteristic, $T(n; \theta_{\max})$:

$$\frac{T_f}{T} \rightarrow 1 = 100\%$$

The common characteristic is nonlinear increasing curve, and natural torque family curves have maximums. Increase of performance is greater at higher engine speeds, where it's necessary for them to be. (Natural reaction of driver who desires greater intensity of vehicle acceleration, is "stronger" accelerator pedal pressure resulting in driving with higher engine speeds).

Controlling vehicle acceleration along acceleration function achieves

- Increase in engine performance,
- vehicle acceleration control without driver.

3. DEFINING ENGINE TORQUE CURVE FAMILY

Engine torque curve family is defined by

$$T = T(n; \theta_i)$$

Acceleration function curve $\varphi_{\max}(n)$ intersects torque curve family $T(n; \theta_i)$.

3.3 OBTAINING CURVE FAMILY

For vehicle, only external torque and power curve is available in the form of smooth curves ("polished" version). The curve families with partial charges are unavailable even for the stationary state. The family of curves during vehicle acceleration (unsteady state, "transients") are unavailable. Determination them is complicated and expensive, and vehicle performance during acceleration is reduced: Part of engine torque is spent on accelerating translationing and rotating masses, [8,9], and the engine speed changes, resulting in less efficient combustion cycles.

There are test benches for determining speed characteristics with software that simulate influence of mass on vehicle acceleration [10]. In the end, actual performance must be determined while the vehicle is on the road.

In this study, for determining engine torque curves family during vehicle acceleration, the physical - mathematical model for wheel torque T_f for vehicles with front wheel drive. Through the transmission ratio i , wheel torque is reduced to engine torque T . Throttle angle θ_i for family members is controlled via electronic accelerator pedal signal (ETC).

3.2.1 Physical – mathematical vehicle acceleration model

Figure 8 shows the vehicle (one longitudinal half of it, "bicycle"), which speeds up along a straight line. Front wheel is driving one, rear wheel is non-driving.

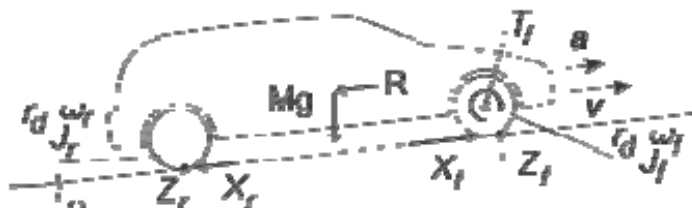


Figure 8: Forces acting on vehicle during accelerating motion

Marks in Figure 8 are:

- T_f – driving wheel torque
- X_f – horizontal road resistance to front wheel (driving wheel tangent reaction)
- X_r – horizontal road resistance to rear wheel (non-driving wheel tangent reaction)
- Z_f, Z_r – vertical road reaction to front and to rear wheel
- R – vehicle movement resistances
- v – vehicle speed
- a – vehicle acceleration
- $\dot{\omega}_f, \dot{\omega}_r$ – angular acceleration of front and rear wheel
- $M=1/2m$ – longitudinal half vehicle mass, m – vehicle mass
- g – gravitational acceleration
- J_f – moment of inertia of one front wheel, and half of drivetrain, clutch and crankshaft
- J_r – moment of inertia of one rear wheel
- r_d – dynamic wheel radius
- α – climbing angle

(All basic and derived measurement units of physical quantities and their designation are SI)

Recording $T(n)$ engine torque family curves is performed on a horizontal road:
 $\alpha=0 \rightarrow \sin\alpha=0, \cos\alpha=1$

Torque balance of front and rear wheel are given in equations (1) i (2):

$$T_f - X_f r_d = J_f \dot{\omega}_f \quad (1)$$

$$X_r r_d = J_r \dot{\omega}_r \quad (2)$$

Angular acceleration values $\dot{\omega}_f, \dot{\omega}_r$ of front and rear wheel are known, due to measuring angular speeds ω_f i ω_r during time t .

Adding equation (1) to (2), the torque balance of front and rear wheel is obtained

$$T_f - (X_f - X_r)r_2 = J_f\dot{\omega}_f + J_r\dot{\omega}_r \quad (3)$$

In equation (3) tangent reaction difference $X_f - X_r$ is unknown because tangential reactions itself are unknown. In order to eliminate tangent reactions X_f and X_r horizontal forces balance equatoions (4) is:

$$Ma = X_f - X_r - R \quad (4)$$

Unknown vehicle acceleration a is determined by angular acceleration $\dot{\omega}_r$ of rear wheel:

$$a = r_2 \dot{\omega}_r \quad (5)$$

Substituting acceleration a from expression (5) into equation (4) eliminates the unknown acceleration a from (4) and gives:

$$Mr_2\dot{\omega}_r = X_f - X_r - R \quad (6)$$

Evaluating (6) tangent reaction difference $X_f - X_r$ is obtained as:

$$X_f - X_r = Mr_2\dot{\omega}_r + R \quad (7)$$

Substituting (7) into (3) torque equation (8) is obtained, in which front wheel torque T_f and vehicle motion resistance R are unknown values:

$$T_f - (Mr_2\dot{\omega}_r + R)r_2 = J_f\dot{\omega}_f + J_r\dot{\omega}_r \quad (8)$$

Although front and rear wheel angular velocities are known (they are measured), to simplify equation (8) assumption (9) are introduced:

$$\omega_f = \omega_r \xrightarrow{\text{yields}} \dot{\omega}_f = \dot{\omega}_r \quad (9)$$

When introducing connections (9) a small error is made: The front wheel rotates at higher speed than the rear one, because the twisting and sliding of drive wheel tire is greater due to front wheel driving torque T_f . In addition, the drive wheel and non-wheel drive sliding is in opposite direction.

However, experiments have shown that the error that appears made by assumption (9) is without affecting the result.

Using assumption (9) torque equation (10) is obtained:

$$T_f - (Mr_d \omega_f + R)r_d = (J_f + J_r)\omega_f \quad (10)$$

According to [6,7] the inertia moments J_f, J_r , can be replaced with

$$I = J_f + J_r = \frac{1}{2} (1 + \delta_1 i_g^2 + \delta_2) [kg \cdot m^2]$$

δ_1 – influence ratio of engine and clutch rotating masses

δ_2 – influence ratio of drivetrain rotating masses

i_g – gear selected for vehicle motion

By solving equation (10):

$$T_f - R \cdot r_d = (Mr_d^2 + I)\omega_f \quad (11)$$

In equation (11) is $R \cdot r_d$ torque resistance T_{fR} to vehicle motion:

$$T_{fR} = R r_d \quad (12)$$

By introducing (12) into (11) gives:

Torque equation for vehicle driving wheel

$$T_f - T_{fR} = (Mr_d^2 + I)\omega_f \quad (13)$$

To transform torque from vehicle wheel to engine, torque (14) and angular velocity relations (15) are introduced:

$$T = \frac{T_f}{i}, T_R = \frac{T_{fR}}{i} \quad (14)$$

$$\omega_f = \frac{\omega}{i} \xrightarrow{\text{yields}} \omega_f = \frac{\omega}{i} \quad (15)$$

i – total transmission gear ratio [-]

With introduction of relations (14) and (15) into (13):

$$i(T - T_R) = (Mr_d^2 + I)\frac{\omega}{i} \quad (16)$$

Relation between circular frequency of angular velocity [rad] and engine speed [o/s] is

$$\omega = 2\pi n \xrightarrow{\text{yields}} \dot{\omega} = 2\pi \dot{n} = 2\pi \frac{dn}{dt}, \quad n \left[\frac{o}{s} \right] \quad (17)$$

With introduction of relation (17) into (16) gives:

Rate of change dn/dt of engine speed n during vehicle acceleration

$$\frac{dn}{dt} = \frac{e}{2\pi(nr_d^2 + j)} (T - T_R) \quad (18)$$

- T – engine torque
- T_R – torque resistance to vehicle motion, transformed to engine
- $T - T_R$: torque difference between engine torque and resistance torque, that remains for vehicle acceleration a

Engine speed n during vehicle acceleration is measured by engine speed sensor and rate of change dn/dt is calculated (which is explained in paragraph 4.2)

From equation (18) by calculation follows:

Engine torque T for vehicle acceleration

$$T = \frac{2\pi(nr_d^2 + j) \frac{dn}{dt}}{e} + T_R \quad (19)$$

Engine torque $T_R = T_{fR}/i$ due to vehicle motion resistance at constant velocity $v = \text{const}$, when influence of inertia is not present, $dv/dt = 0$, is related to external environment. It occurs on the path – road that vehicle passes. It consists of air drag torque T_{drag} , rolling resistance torque T_{roll} and climbing resistance torque T_{climb} [8,9]:

$$T_{fR} = T_{drag} + T_{roll} + T_{climb} \quad (20)$$

- $T_{fR} = R \cdot r_d$ – torque resistance to motion
- R – resistance to vehicle motion
- r_d – dynamic wheel radius

Total motion resistances R are given by expression (21), [8,9]:

$$R = R_{drag} + R_{roll} + R_{climb} \quad (21)$$

where particular resistance is given as

- $R_{drag} = KAv^2$ – aerodynamic resistance force [N]
- $R_{roll} = Gf_{roll} \cos \alpha$ – rolling friction resistance [N]
- f_{roll} – Coefficient of rolling resistance [-]
- $R_{climb} = G \sin \alpha$ – grade resistance [N]

Using particular resistance expressions, equation (21) turns to

$$R = KAv^2 + Gf_{roll} \cos \alpha + G \sin \alpha \quad (22)$$

4. EXPERIMENTAL RESULTS

Experimental research has been done using vehicle *VW Polo 1.2* engine with computer *SIMOS N9.1*. The vehicle is shown in Figure 9.



Figure 9: Experimental vehicle

4.4 VEHICLE AND TRANSMISSION PARAMETERS (VEHICLE SETUP)

Following data are obtained from reference [9] or arbitrarily chosen according to guidelines presented in reference [9].

Vehicle

- $K=C_x \cdot \rho / 2$ – reduced air drag resistance coefficient [kg/m³]; [7]
- C_x – aerodynamic drag coefficient = 0.30 [-]
- ρ – mass density of air = 1.226 [kg/m³]; [7]
- A – frontal area of the vehicle = 1.75 [m²]
- $G=2Mg$ – vehicle weight [kN], M – mass [kg] longitudinal vehicle half
- $2M=1200$ [kg]
- $g=9.81$ [m/s²] acceleration due to gravity
- $r_d=0.3$ [m] dynamic wheel radius

Drivetrain

- $i = i_0 i_l = 16.01$ [-] – overall transmission ratio
- (i_0 – main drive transmission ratio [-])
- (i_l – first gear transmission ratio [-])

$J=1/2\delta=1/2(1+\delta_1(i_g)^2+\delta_2)$ [kgm²], moment of inertia due to [9]
 $\delta_1 = 0.020$ [kgm²] influence ratio of engine and clutch rotating masses, adopted according to [9]
 $\delta_2 = 0.025$ [kgm²] influence ratio of drivetrain and wheels rotating masses, adopted according to [9]

Total gear ratio is obtained by calculating the ratio of engine to front wheel revolutions:

$$i = \frac{n}{n_f} = \frac{\omega_f}{2\pi} \left[\frac{\sigma}{s} \right] \cdot \omega_f = \frac{v}{r_g} \left[\frac{\text{rad}}{s} \right]$$

Vehicle speed is measured during constant vehicle speed, $v=const$, using satellite navigation device (GPS), and respective number n of engine speed, taken from crankshaft.

For the vehicle speed of $v=25$ [km/h] and its respective engine speed of $n=3545$ [1/min] the overall first gear transmission ratio is calculated to $i=16.04[-]$. The transmission ratio was calculated several times for various sets of values for engine speed and vehicle speed, yielding similar results.

Overall transmission ratio depends on gearbox transmission ratio, which is fixed as design characteristic, and dynamic wheel radius which varies on tire type, size, pressure and wear, as well as vehicle mass distribution on individual wheel. More mass on wheel results in smaller dynamic radius. In order to include all of this influences on dynamic wheel characteristic, overall transmission ratio was calculated using engine speed and vehicle speed and not by simply using technical data for vehicle transmission provided with the vehicle.

4. 5 RECORDING AND PROCESSING DATA FOR TORQUE CURVE ENGINE FAMILY

Torque curve family has been created from records of particular family members that relate to their throttle angle θ_i , with assistance of custom ETC software via microcontroller. The family was recorded for both 1st and 2nd gear, in order to minimize computational errors.

Vehicle accelerated in range (n_{min}, n_{max}) for each engine charge set by throttle angle.

Signals of engine speed n were recorded during time t and its rate dn/dt was calculated according to expression logic (18). Signals were taken from engine speed sensor.

Signal processing yields engine speed n and it's rate of change dn/dt . T_R corresponds to external resistances and is calculated from n and overall transmission ratio as explained below expression (19). Finally, torque T (speed characteristic of engine) is calculated according to expression (19). Note that, according to (18), dn/dt depends on external resistances so they are unavoidably included in the evaluation of dn/dt from measurements.

To process and to transform signal data $n/t \rightarrow dn/dt \rightarrow T(n)$ special software was developed from scratch.

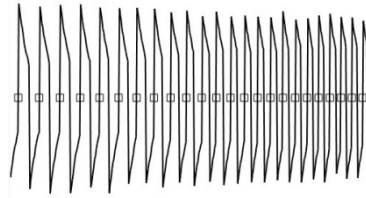


Figure 10a: Raw data of recorded signal

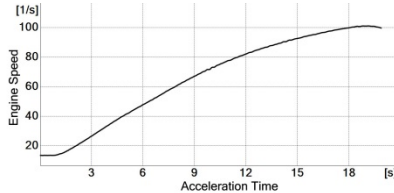


Figure 10b: Engine speed vs time

The algorithm use statistical analysis to identify signal periods from raw data shown in Figure 10a. Small squares displayed in Figure 10a, are not part of signal raw data and they show the result of identification. The program adds this squares automatically. Then, lengths of periods and their time indexes are calculated and transforming into engine speed in time, as shown in Figure 10b. Having the functional dependences of engine speed to time, program then calculates the rate of change of engine speed in time, which is used in expression (19) to calculate torque.

Figure 11 shows torque speed characteristic $T(n)$ obtained by described procedure.

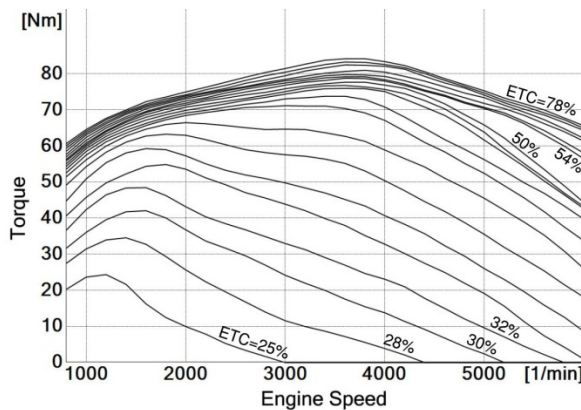


Figure 11: Engine torque family curves

In Figure 11, torque family parameter is the ETC position wich uses values: {78, 74, 70, 66, 62, 58, 54, 50, 48, 46, 44, 42, 40, 38, 36, 34, 32, 30, 28, 25}. ETC positions over 78% do not significantly increase engine torque.

Torque curve maximums for low and middle values $T < 65$ [Nm] are found at lower engine speeds $n < 2000$ [o/min]. Torque curve maximums for values $T > 70$ [Nm] and further toward external characteristic are located in range of revolutions $n = (3500 \div 4000)$ [o/min]. In addition, for torque values $T > 50$ [Nm] there is an accumulation of curves, despite to equal increment step of ETC position of 4%.

Appearance of curves family is a consequence of engine computer remapping.

For lesser engine charges, torque maximums are shifted toward lower revolutions. Shifting suitable operating mode at lower charges to lower engine speed, stimulates the ride at lower revolutions. Higher gear ratios are implicated. It is a matter of fuel consumption optimization and extending engine working life time.

For grater charges maximal performances have to be allowed. However, such a driving is discouraging: The same increase of ETC position in maximal torques domain yields far less torque than the increase in medium and low engine torques (charges). This behavior is achieved due to family curves accumulation in the area of large torques (charges).

(Remapping is introduced from vehicle manufacturer).

After signal data processing and transformation, torque family data are obtained, whose analog form is showed in Figure 11, and its digital form is saved into lookup table.

Common torque family characteristic from Figure 11 is shown in Figure 12.

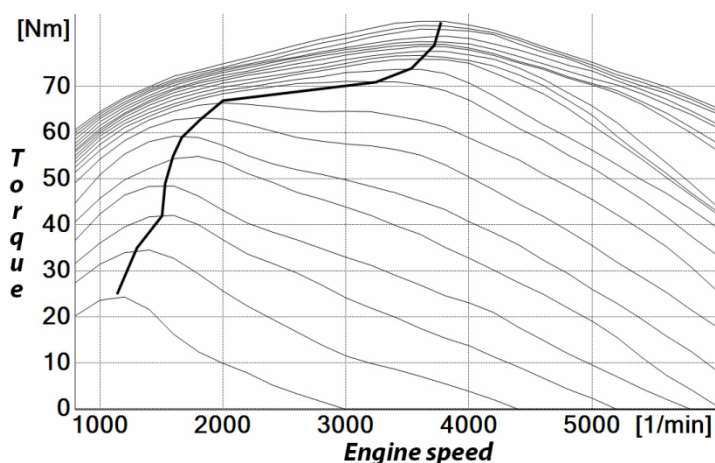


Figure 12: Common torque curve characteristic of experimental vehicle

4. 6 ENGINE CHARGE CONTROLLER AND PROGRAMMING CODE FOR VEHICLE ACCELERATION

In order to control vehicle acceleration new controller (hardware) is developed from scratch. The controller is shown in Figure 13.

Controller intercepts signals of electronic throttle control (ETC) and sends signals to engine control unit (ECU) through which it controls engine charge along acceleration function. The only driver's task is to give starting charge by pressing accelerator pedal.

Engine charge control is conducted by controlling throttle [11], and setting its angle θ . Commonly a feedback loop [12] is used (i.e. PI regulation).

Lack of feedback loop control regulation is angle oscillations, $\pm\Delta\theta$ of throttle valve flap, which occurs around controlled angle θ_i , due to error compensation during engine torque regulation [13]. Throttle flap oscillations cause unsteady state of engine charge, therefore fuel consumption rises and exhaust gas composition especially gets worse.

In solution shown in this study throttle valve flap oscillations do not exist.

Controller work information is current engine speed. As revolutions increase in small steps (increment) flap grows, too. Change is smooth and only in the direction of angle increase.

There are two more acceleration functions for which the controller can perform vehicle acceleration: One prevents excessive torque that causes drive wheels to spin on the slippery road, and the other increases passenger comfort changing acceleration characteristic and controlling its intensity. Showing of results obtained with these features is a topic for another paper.



Figure 13a: Torque controller

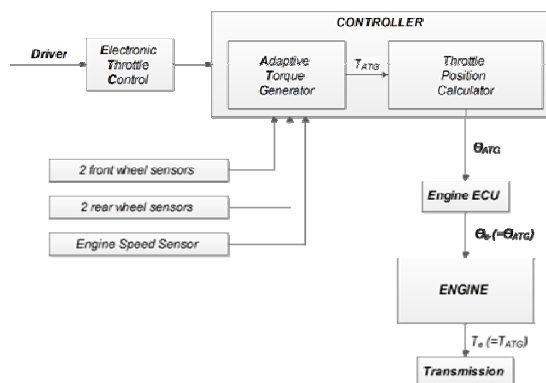


Figure 13b: Block diagram of Torque controller

Figure 13b, Block diagram, explanation:

- *Driver*: Sets desired *ETC* position
- *ETC*: Transmits signal to *Controller*
- *Controller*: Determines engine torque T_{ATG} and its corresponding throttle valve angle θ_{ATG} and sends it to *Engine ECU*
- *Engine ECU*: Sets throttle valve angle θ_e to calculated value θ_{ATG}
- *Engine*: Produces engine torque T_e which value is T_{ATG} and delivers it to the *Transmission*
- *Feedback*: Current engine speed is sent back to *ATG Controller*

Figure 13b shows control flow diagram of vehicle acceleration. During acceleration, the driver sets desired engine torque using accelerator pedal, ETC. Controller successively modifies signals sent to ETC according to maximal engine torque efficiency acceleration function $\varphi_{\max}(n)$ and relays them to engine computer, ECU. Engine computer gradually opens throttle valve, engine torque increases and vehicle accelerates. Current engine speed is feeded into controller and it is used for successive increase of throttle valve angle in real-time. Controlled acceleration ends when the engine reaches torque desired by driver. Wheel speed sensors shown in Figure 13b are used in case the vehicle starts to skid (mostly on slippery road) in conjunction with another acceleration function to prevent transmission of excessive engine torque to wheels.

4. 7 NUMERICAL CONTROL OF VEHICLE ACCELERATION

For controller operation, two new programs are developed from scratch, one to control and one to execute (software).

Control code includes Control functions for acceleration (logic), and is written in the programming language C Sharp (C #). Control code passes data to executive code.

Executive code includes Executive instructions for acceleration (execution), and is written in the programming language C. The code passes data to engine control unit (ECU) for throttle valve angle flap.

Two codes are connected through external link for data communication.

Numerical acceleration control by programming code accelerates vehicle along acceleration function in such a way that torque T_e values correspond to maximal torques of partial engine charges θ :

$$T_e = \varphi_{\max}(n)$$

T_e – engine torque on common characteristic curve

n – engine speed, acceleration function parameter

Note that acceleration function calculates torque for common characteristic curve from engine speed.

First step is finding torque T_e , on common characteristic family curve for actual number n of revolutions:

$$n, \varphi_{\max} \xrightarrow{\text{lookup}} T_e$$

Second step is finding throttle valve flap angle θ for actual number n of revolutions and torque T_e on common characteristic family curve:

$$n, T_e \xrightarrow{\text{lookup}} \theta$$

Valve flap angle θ determines member θ_i of torque family that intersects common characteristic family curve at engine speed n .

Torque family is digitalized and stored in lookup table.

Calculation procedure is repeated as number n of revolutions increments in time t .

4. 8 EXPERIMENTS WITH VEHICLE ACCELERATION BY ACCELERATION FUNCTION

When the driver presses accelerator pedal, controller takes control over engine charge. Development of torque does not go beyond its natural curve $T(n;\theta_i)$, instead it follows curve $\varphi_{\max}(n)$ of acceleration function:

$$T = \begin{cases} \varphi_{\max}(n), & T(n, \theta_i) > \varphi_{\max}(n) \\ T(n, \theta_i), & T(n, \theta_i) \leq \varphi_{\max}(n) \end{cases}$$

Vehicle acceleration along acceleration function ends in the intersection point of natural engine curve $T(n;\theta_i)$, and acceleration function curve T . Engine charge for natural curve is determined by throttle valve flap angle $\theta_i(h)$ – for selected position h of accelerator pedal.

Figure 14 shows vehicle acceleration curve along acceleration function $\varphi_{\max}(n)$ of maximal engine effectiveness for external torque characteristic, $\theta_{\max}(h_{\max})$. The curve is recorded while driving in 2nd gear, i2. Oscillatory appearance of curve is result of noise in the signal. In reality there are no flap oscillations, because changes of throttle valve angle are incremental and with small step.

By remapping engine control unit (ECU) the nature of torque family has been changed, so that instead of just one maximum, curves have two local maximums near to torque value $T(n=2500)=60$ [Nm]. Therefore the program that controls acceleration does not function with the expression given nearby Figure 6, where throttle valve flap angle θ_i for maximum torque curve determines partial function derivate to number n of revolutions:

$$\theta_i: \frac{\partial T}{\partial n}(n; \theta_i)$$

Instead, program functions with the expression:

$$\phi_{\max}(n) = \left\{ T(n; \theta_i) \mid \theta_i: T(n; \theta_i) = \max_n T(n; \theta_i) \right\}$$

According to the previous expression flap angle θ_i is such that for fixed value n the corresponding torque curve value is exact as its maximum value on the whole engine speed range.

$$\theta_i: T(n; \theta_i) = \max_n T(n; \theta_i)$$

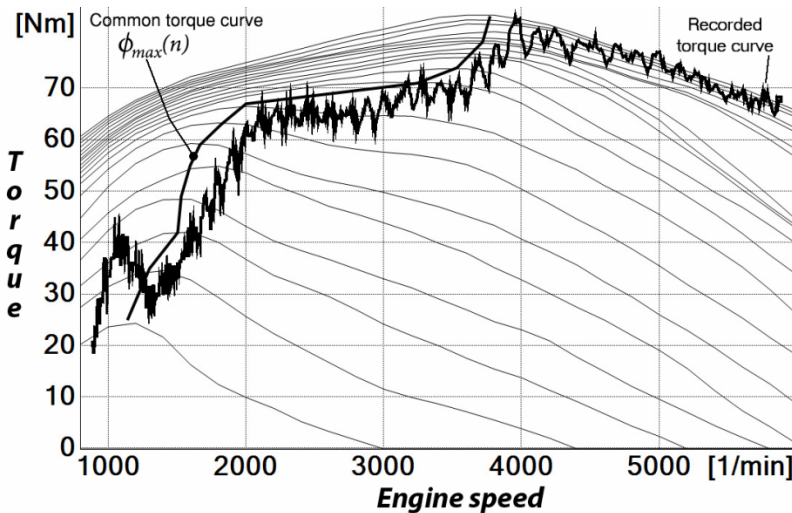


Figure 14: Torque curve recorded during vehicle acceleration vs Common torque curve characteristic

The common torque curve is used as an acceleration function and recorded torque curve in Figure 14 is real acceleration curve which is a result of controlled acceleration using acceleration function.

The recorded acceleration curve, shown at Figure 14, is obtained exactly as the torque curve family were obtained using expression (19) and signal processing.

4.5.1 Flow of acceleration curve

Vehicle was accelerating longitudinally, i.e. along straight line on horizontal road in 2nd gear from $n=n_{min}\sim 800$ [1/min] to $n_{max}=6000$ [1/min]. Engine has electronically limited maximum speed of $n=n_{max}$. At engine speed $n=6000$ [1/min] vehicle reaches the speed of $v=90$ [km/h].

At the beginning vehicle is moving at a constant minimum speed, $v=const$, $n_{min}=const$, and accelerator pedal is set to default position $h=h_{min}$ (not pressed). Recording starts the moment the accelerator pedal has been suddenly pressed to its maximal position $h=h_{max}$. Engine speed rises from $n\sim 800$ [o/min] to $n\sim 1100$ [1/min] followed by torque rise to a value of $T\sim 40$ [Nm]. During that time controller makes calculations for values of n and θ_i for the beginning of acceleration.

In the range $n\sim(1100$ [1/min] \div 1350 [1/min]) controller reduces charge (engine load) and engine torque decreases to minimal value of $T\sim 27$ [Nm]. From that point engine starts to follow acceleration function $\varphi_{max}(n)$.

From $n\sim 1350$ [1/min] to $n\sim 3700$ [1/min] the controller follows common characteristic curve.

At $n\sim 3770$ [1/min] controller leaves acceleration function $\varphi_{max}(n)$ and engine reaches external speed characteristic of torque curve whose $T_{max}\sim 80$ [Nm].

Up from $n\sim 4000$ [1/min] ends control and further vehicle acceleration is taking place on the natural curve torque $T(n;\theta_{max})$. Throttle valve flap angle reaches $\theta_i=\theta_{max}$, control of accelerator pedal signals stops and pedal control is returned to driver, who keeps accelerator pedal pressed down to the floor, all the time. (However, safety measures make it possible that control of vehicle motion to be returned to the driver immediately at any moment).

Record of acceleration curve shows that controller optimizes torque rise in range $n=(1600\div 2000)$ [1/min], deviating minimally from common characteristic curve and also at $n=3770$ [1/min]. Following strictly common characteristic would demand rapid changes of $\alpha=da/dt$ and a acceleration, which is undesirable, because it will result in increase in fuel consumption and worse composition of exhaust gases.

4.9 ENERGY CONSUMPTION

Otto engine uses mixture of fuel and air whose ratio varies within very small range. In homogenous engine operation, for experimental vehicle, so called "ideal mixture" is used which has excess air coefficient $\lambda=1$ [-]. Fuel is injected into the intake pipes, while the exhaust system has a three way catalytic converter for exhaust gases neutralization only (no converters for nitrogen oxides, which is typical for operation with poor mixture, $\lambda<1.05$). Also, the engine does not have a valve for exhaust gas recirculation, EGR.

Mixture composition where $\lambda=1$ is stoichiometric, where for combusting 1 [kg] of fuel, 14.7 [kg] of air is used.

During acceleration ECU may enrich the mixture by $1-3\%$ ($\lambda=0.97-1.00$) which deviates from "ideal mixture" in order to speed up fuel combustion. Mixture enrichment depends on acceleration intensity. The greater the acceleration, the richer the mixture is.

Acceleration intensity during uncontrolled acceleration is greater than during controlled acceleration, where the fuel consumption is lower on basis of mixture composition. Therefore, the fuel consumption can be taken as proportional to air mass flow under assumption that mixture composition is the same during both controlled and uncontrolled acceleration, $\lambda_c=\lambda_u$.

The air mass consumption was measured in time using hot film air mass meter “HFM5”, [12], Figure 15b. Data were taken during acceleration (2^{nd} gear, overall transmission ratio $i=8.68$) where engine speed ranges from $n=850$ [1/min] to $n=5500$ [1/min]. For comparing consumed air masses, engine speed range from $n=1140$ [1/min] to $n=3770$ [1/min] is selected, since maximal engine torque efficiency acceleration function is defined in that range. For both controlled and uncontrolled acceleration, accelerator pedal ETC was pressed rapidly to its maximal position and held down during the whole acceleration.

Data from sensor was captured using two-channel oscilloscope “PICO” for car engines and recorded to a “csv” file, which computer program uses as an input for processing.



Figure 15a: Air mass meter and intake hose installation setup



Figure 15b: Air mass meter closeup

To reduce disturbance as much as possible, a long intake hose (white) is installed as shown in Figure 15a. Air enters air mass meter first, then flows through the hose toward throttle valve. Hose length and hose bends reduce energy of disturbance travelling to measurement device.

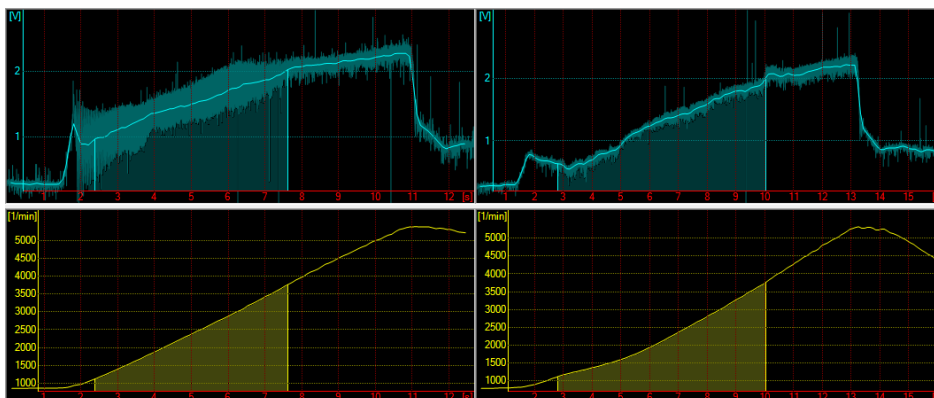


Figure 16: Air flow data (top) and engine speed (bottom) in time during uncontrolled (left) and controlled (right) acceleration

Top images in Figure 16 show graphical representation of data taken from air mass meter as voltage in time. The bright smooth curve is a result of processing the raw data numerically in order to eliminate noise. The noise in raw data is a result of disturbance in

the air flow induced while opening and closing the intake valve. This noise is greater during uncontrolled acceleration because the throttle valve is wide open (WOT). During controlled acceleration, throttle valve is less open and it acts as a barrier for the air flow wavefronts, resulting in significantly less disturbance.

From 1.5s to 2.0s, the air flow curve has a characteristic rise as a consequence of sudden opening of the throttle valve. The air rapidly fills the intake pipe behind the throttle valve toward intake valves, where afterwards engine starts air suction, causing the air flow curve to decline. After that, the air flow curve is continuously rising as the engine speed is increasing.

Total air mass m consumed and distance travelled S during both controlled and uncontrolled acceleration are:

$$m = A \cdot k, \quad A = \int_{t_1}^{t_2} U(t) dt$$

$$S = N \cdot i, \quad N = \int_{t_1}^{t_2} n(t) dt$$

- $U(t)$ – air mass flow curve (obtained by processing air flow data) [V]
- t_1, t_2 – time indexes at which the engine speed is at 1140[1/min] and 3770[1/min]
- A – area below $U(t)$ from t_1 to t_2 (shaded area in Figure 16, top sections) [Vs]
- k – constant of ratio between mass m and A [kg/Vs]
- m – total mass of air flown through the air mass meter [kg]
- $n(t)$ – engine speed in time (curves in bottom sections of Figure 16) [1/min]
- N – area below $n(t)$ which is total number of engine revolutions between t_1 and t_2 [-]
- i – overall transmission ratio [-]
- S – total distance travelled [m]

The effect of controlled acceleration on energy saving E is obtained by calculating ratio between average air mass flows over their respective distances, m_c/S_c for controlled and m_u/S_u for uncontrolled:

$$E = \frac{\frac{m_c}{S_c}}{\frac{m_u}{S_u}} = \frac{\frac{A_c \cdot k}{N_c \cdot i}}{\frac{A_u \cdot k}{N_u \cdot i}} = \frac{\frac{A_c}{N_c}}{\frac{A_u}{N_u}} = \frac{I_c}{I_u} [-], [%]$$

I_c, I_u – indicators of air (fuel) consumption reduced to travelled distance for controlled, c , and uncontrolled, u , acceleration [Vs]

Note that calculation of E is independent of selection of constants k and i to be known.

4.6.1 Experimental results

Several sets of data was collected, compiled and ordered into a table below.

Table 1: Experimental data with effectiveness calculations

	t_0 [s]	t_1 [s]	Δt [s]	A [Vs]	N [-]	$I=A/N$ [Vs]
Controlled	2.805	10.019	7.214	9.133037	264.87	0.034481
Uncontrolled	3.057	7.601	4.544	7.184566	190.01	0.037812
Ratio	-	-	159%	127%	130%	$E = 91%$

Note: Values A and N are computer calculated

Table 1 shows that duration Δt of controlled acceleration is 59% greater than duration of uncontrolled acceleration and that is due to lower engine torque during controlled acceleration. Area A , which reflects total air masses consumed, is 27% greater during controlled acceleration, while the total number of engine revolutions N , which reflect travelled distance, is 30% greater during controlled acceleration.

Indicators $I=A/N$ of air (fuel) consumption show that $I_c < I_u$ ($0.034481 < 0.037812$), which means that controlled acceleration consumes less fuel than uncontrolled one.

Effectiveness $E=I_c/I_u=91%$ shows that 9% of the fuel is saved during controlled acceleration for the same starting and ending engine speed, thus the same starting and ending vehicle speed.

5. CONCLUSIONS

Researchers make continuous efforts to improve vehicle fuel economy and reduce their impact on the environment. Measures for reducing fuel consumption are transferred to the control of movement, and in particular to control vehicle acceleration. Vehicle acceleration takes up to 40% of total fuel consumption. Significant fuel savings, >25% are made just with smooth drive, by constant speed, $v=const$.

However, the vehicle is inevitably moving with variable speed. Changing vehicle speed means vehicle acceleration, $a=dv/dt$, and transition to acceleration movement changes the way of acceleration, $\square=da/dt=d^2v/dt^2$.

The usual reduction in fuel consumption is achieved by the formula:

"Reduction of torque + delay in responding to pedal pressure."

Acceleration a is controlled by reducing torque. The "Torque map" is reprogrammed on relation *accelerator pedal movement – number of revolutions – engine torque*. Frequently for original mode of operation two different modes are added, resulting in a three-level control with the exclusive choice.

By reducing torque vehicle performance are reduced.

Delayed response of the throttle controls acceleration change \square of acceleration a . The delay in the response of accelerator pedal is realized by software modification of electronic throttle control (ETC) signals.

Slow response to the accelerator pedal pressure reduces car driveability.

This paper presents study results of vehicle acceleration control by numerical engine torque control in function of acceleration.

Inevitable formula of torque reduction and throttle response delay for acceleration control a and acceleration rate \square is applied. However, the approach is different: Maximum engine torque efficiency used at relation *accelerator pedal movement – number of revolutions – engine torque*.

With this approach, the loss of the vehicle's performance is minimal. Regulation of torque impairment is single stage, continuous and progressive: Vehicle performance and responsiveness to accelerator pedal position change increase as engine speed increases.

Torque family is the starting information used to control engine torque.

To supply a torque family in transitional period special physical - mathematical model is developed. Based on the model, individual family members are captured during vehicle acceleration on the road. This takes two important influential factors into account:

- Reducing vehicle performance due to reduced engine torque caused by inertia resistance
- Engine effectiveness decrease due to of variable engine working speed

Using the common torque characteristic curve, which passes through torque maximums of family members, a function along which guided engine torque during vehicle acceleration is created. Natural engine torque curve is replaced by a curve with a maximum torque effectiveness. This increases the effectiveness of vehicle acceleration.

To control the acceleration, controller (hardware) and program (software) are designed. Programming code reads data from torque family table. The table stores digital data on the size of the torque, depending on engine speed for the family members. Each member of the torque family represents engine charge determined by throttle valve flap angle.

The program calculates the required torque magnitude for acceleration function and current engine speed. For calculation numerical methods are used, interpolation and advanced programming techniques. The results of the program calculation are passed to controller, which via executable code controls throttle valve in order to charge engine.

By given solution at lower speeds fuel savings are greater, but performances are inevitably reduced. Inverse is also true: With speed increase fuel savings decreases, but performances rise.

Here presented system interacts with driver. The driver determines the starting and ending engine speed by increasing position of accelerator pedal. Choosing the engine speed range for acceleration of the vehicle driver affects vehicle performance and fuel economy. Higher engine speed ranges provide better performance at the higher cost.

Idea of the concept is preliminary tested on the computer, before the concept is tested in practice. For this purpose a special simulation software is developed.

Experimental results show that energy consumption reduced to travelled distance has efficiency $E=91\%$ by controlled acceleration compared to uncontrolled acceleration, so that energy saving is 9%. Because of lower acceleration intensity, time to reach the same engine/vehicle speed is 59% greater during controlled acceleration then during uncontrolled one, but during grater time, travelled distance is as well 30% greater.

Energy (fuel) saving is realized due to:

- Controlled acceleration along the maximal engine torque efficiency function
- Reduced inertia resistance as a result of lower acceleration rate

Any driver can save fuel using this method because it relies on technical means, which are irrelevant to driving style.

Vehicle experiments confirmed possibility to increase engine efficiency while accelerating vehicle via numerical control by acceleration function.

6. REFERENCE

- [1] Hofmann D. at all – „Gasoline Engine Management“, Robert Bosch GmbH 3rd edition 2006
- [2] Belingardi G., Obradović J. – „Recent development in car body lightweight design – a contribution toward greener environment“, *Mobility & Vehicle Mechanics*, Vol. 38 No 4, 2012
- [3] Fuji Heavy Industries Ltd. – http://drive2.subaru.com/Summer07_whatmakes.htm, “It's What Makes a Subaru, a Subaru: Subaru Intelligent Drive (SI-DRIVE)”, last accessed on February, 6. 2013.
- [4] Press Information: Fuji Heavy Industries Unveils the Revolutionary Intelligent Driving Enhancement System “SI-DRIVE”, Tokyo, April 14, 2006
- [5] Technicians Reference Booklet, MSA5P0161C, “Fuel Injection and Engine Management” Module 406, Subaru of America Inc. 2007. page 77.
- [6] Ford Motor Company – http://media.ford.com/article_display.cfm?article_id=33965 „ALL-NEW FORD FOCUS FEATURES ECOMODE TO HELP DRIVERS PERFECT ECO-DRIVING TECHNIQUES“ Ford Motor Company Newsroom, last accessed on February, 8. 2013.
- [7] Friedrich K. and others – „Safety, Comfort and Convenience Systems“, Robert Bosch GmbH 2006
- [8] Simić D. – “Motorna vozila”, (in transl. „Motor vehicles“), Naučna knjiga (in transl. „Science book“), Belgrade 1977
- [9] Janković D., Ivanović G., Todorović J., Rakičević B. – „Teorija kretanja motornih vozila“ (in transl. „Vehicle motion theory“), Faculty of mechanical engineering in Belgrade 2001
- [10] Joly P., Duboc S. – „Common Rail Mapping on Power train Test Bench“, Technical Paper F2000 A054, Proceedings of Seoul 2000 FISITA World Automotive Congress 2000, Seoul, Korea, June 12-15 2000
- [11] Deur J, Paković D., Burgio G., Hrovat D. – „A Model Based Traction Control Strategy non-reliant on wheel sleep information“, *Mobility & Vehicle Mechanics*, Vol. 49 No 8, 2011
- [12] Jae-Book S., Byong-Cheol K., Dong-Chul S. – „Development of TCS Control Logic Based on Engine Throttle Control“, *Journal of mechanical science and technology*, Vol. 13 No 1
- [13] Minsuk S., Yaehyun K., Yeamyoun Y., Myuongho S. – „Design of a network based traction control system using a formalized design procedure“, FISITA F2006SC22 2006
- [14] Mencher B. at all – „Automotive Electrics Automotive Electronics“, Robert Bosch GmbH 5th edition 2007

¹ INVESTIGATION OF VIBRATORY LOADINGS OF MOTOR VEHICLE'S USER IN OPERATION CONDITIONS

Miroslav Demić, Jovanka Lukić, Živorad Milić

UDK: 629.18; 534.1; 614.872

Summary

Investigations of a human body behavior exposed to whole body vibration of vehicles are important in design phase of vehicles. Results make possible to model human vehicle oscillatory system and vehicle parameter optimization from ride comfort aspects. Experimental results of investigations of motor vehicles users vibratory loads (passengers and duty) depending on operational conditions (road surface, vehicle speed). Obtained results were base for further investigation of human body behavior exposed to whole body vibrations in laboratory conditions.

Key words: human, whole body vibration, vibratory loads, random vibration

ISTRAŽIVANJE OSCILATORNIH OPTEREĆENJA KORISNIKA MOTORNIM VOZILA U EKSPLOATACIONIM USLOVIMA

UDK: 629,18; 534,1;614,872

Rezime

Istraživanje ponašanja čovečijeg tela pod dejstvom vibracija u vozilu su od izuzetnog značaja za projektovanje motornih vozila. Ona omogućuju modeliranje oscilatornog sistema čovek-vozilo i optimizaciju parametara vozila sa aspekta oscilatorne udobnosti. U radu su prikazani rezultati eksperimentalnih istraživanja oscilatornih opterećenja korisnika pri korišćenju vozila (putnička, teretna) u zavisnosti od eksploatacionih uslova (vrsta puta, opterećenje vozila, brzina kretanja vozila). Dobijeni rezultati su bili osnova za istraživanje ponašanja čoveka pod dejstvom vibracija u laboratorijskim uslovima – na pulzatoru

Ključne reči: human, whole body vibration, vibratory loads, random vibration

¹ *Received March 2013, Accepted: June 2013.*

Intentionally blank

INVESTIGATION OF VIBRATORY LOADINGS OF MOTOR VEHICLE'S USER IN OPERATION CONDITIONS

Miroslav Demić¹, Ph.D, Full professor, Jovanka Lukić, PhD, Full professor, Živorad Milić, Phd,ME

UDC: 629,18; 534,1;614,872;629.1.07

1. INTRODUCTION

Investigations of a human body exposed to vibratory loads are significant in vehicle design. It enables modelling and parameters optimisation of vehicles from ride comfort aspects. In order to obtain reliable laboratory conditions experiment in operational conditions are conducted. Passangers and trucks are used in experimental conditions.

Users of vehicles are exposed to broadband random vibration in longitudinal, lateral and vertical directions, as well as angular oscillatory loads. Field experiments are conducted in the first phase of investigations in order to get data about dominant vibratory loads of human in motor vehicle.

The influence of vertical vibration on human is analysed in significant number of published papers, because oscillatory loads are highest in vertical direction [4,15-16]. The influence of the multi-axial vibrations is not investigated in such number of papers. In order to determine the influence of multi-axial vibrations on human it was necessary to rang vibratory load directions in passenger cars and trucks in operational conditions. Field experiments were conducted.

2. EXPERIMENTAL RESEARCH OF ACTUAL VIBRATORY LOADS OF HUMAN IN VEHICLES

Data about dominant vibratory loads of passengers are important for parameter identification of ride comfort of vehicle. Field experiments are conducted in operational conditions. Accelerations in three orthogonal directions are measured (fore and aft x , lateral y and vertical z), according to [18-20] on seat and floor of the vehicle in order to determine dominant vibratory loadings of passengers. Inductive accelerometers HBM B12/200, amplifier HBM DMC 100 and data acquisition software BEAM 3.1 (Apple Macintosh operating system) are used. Each record lasted $T=27.33$ s, number of data points was $n=2048$ and data acquisition step was $\Delta t=1.33*10^{-3}$ s. Spectral analysis was performed in the frequency domain of 0.09-37.5 Hz. Each factor level was repeated $N=5$ times.

Experiments were performed on good and bad asphalt road. Acceleration signals in "good asphalt conditions" are recorded on straight-line section of road Kragujevac-Batočina. Accelerations signals in "bad asphalt conditions" are conducted on flat horizontal section of "old road" Kragujevac-Batočina between Maršić i Korman turns. Lane had small number of holes.

Different types of passenger cars were used: Yugo 65 cl, Florida equipped with standard vehicles suspension system, Florida equipped with prototype of new suspension

¹ Miroslav Demić, University of Kragujevac, Faculty of Engineering, demic@kg.ac.rs

system and Fiat Croma, as well trucks: Rival, Turbo Zeta and Euro Cargo. All vehicles both passengers and trucks were new.

Measurements were conducted in three speed regimes: 30, 60 and 90 km/h. Vehicle's speeds was constant.

Trucks were loaded and unloaded and had speed 30, 50 and 70 km/h on good and bad asphalts.

Chosen roads represent road network in Serbia and chosen speeds are adapted to road conditions. Time series of accelerations are recorded under constant speed conditions in order to get stationary ergodic random process.

Computer memory limitation caused repeating of measuring five times and total time signal was 135 s. Recorded time signals of accelerations are analysed by using of Macintosh Powerbook 150 and software BEAM.

Accelerometers measuring positions were on the floor below seat and on the seat cushion of assistant driver are given in figure 1. The measuring points were the same both passenger cars and trucks. Measurement set up is given in figure 2.

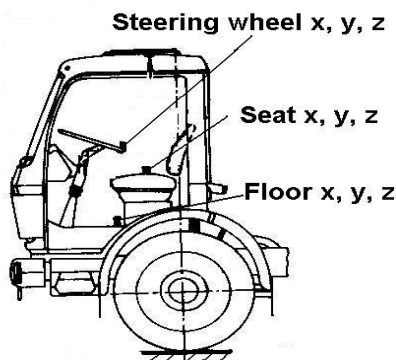


Figure 1 Measuring points

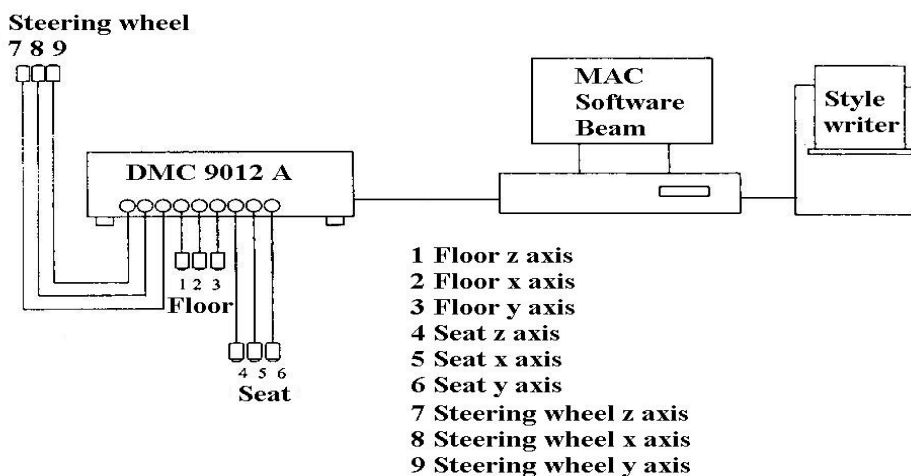


Figure 2 Measurement set up

Time series of accelerations measured in vehicle 4910H on different roads are random signals and are given in figure 3.

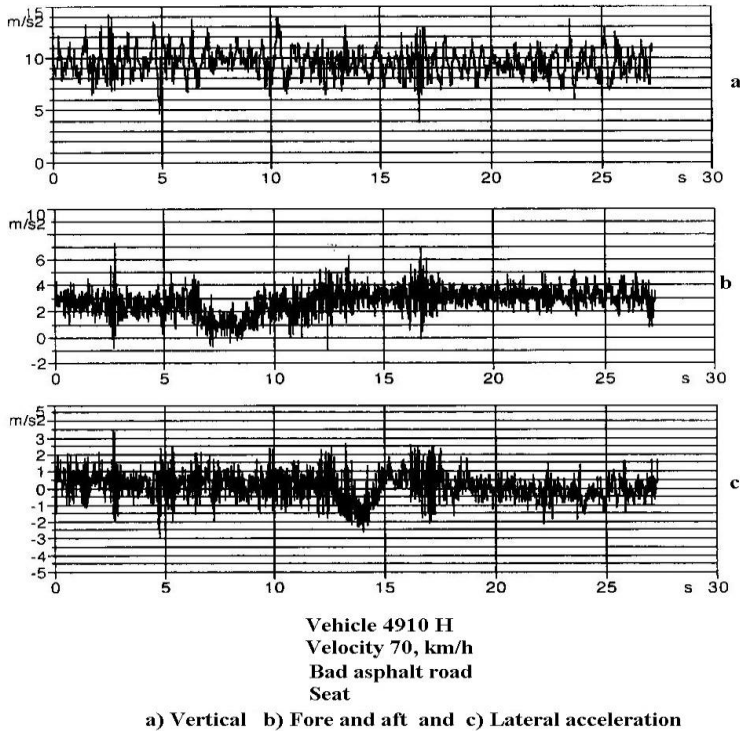


Figure 3 Seat vibration of vehicle 4910H driven on bad asphalt road, vehicle speed was 70 km/h: a-vertical, b-fore and aft and c-lateral direction

3. DATA ANALYSIS

Procedure of data analysis depending on testing vehicle will be given in this chapter. [11][12].

3.1 PASSENGER CARS

Experimental research included more different influencing factors which should be analysed in detail. Preliminary analysis showed that all recorded signals are random and statistically methods should be applied, [9].

Root mean square values of accelerations (R.M.S.) are significant value for ride comfort assessment, [7] except in case that crest factor is less 6, and higher than 9, according to ISO 2631/1 recommendation, [7]. The influence of some factors on human's vibratory loads are investigated by application of acceleration r.m.s. Measured r.m.s. accelerations are normalized and are weighted according to ISO 2631/1 [7].

Average value, r.m.s. value and standard deviation of acceleration signals are determined. Random error, caused by random signal of limited duration, is determined

according to, [3]: $\varepsilon_r = \frac{\sigma_x}{\mu_x \sqrt{n}}$, and is between $4.07 \cdot 10^{-4}$ and 0.0256 []. Random error

caused by determination of r.m.s. values, [3] is : $\varepsilon_r = \sqrt{\frac{2}{n}}$ and its value is 0.03125 []. Crest

factor for all measurement is between 1.04719-3.0769 [], which is satisfactory condition defined in [35].

Experimental results are analysed by analysis of variance method for factorial experiment. Four factors are analyzed (*road surface, vehicle speed, vehicle model and acceleration direction*), and are given in Table 1.

Table 1 Experimental factors

Factor	Number of factor level	Factor level
A – road	a=2	1 - good asphalt 2 - bad asphalt
B – speed	b=3	1 - 30 km/h 2 - 60 km/h 3 - 90 km/h
C – vehicle model	c=4	1 - Fiat Croma 2 - Florida, serial suspension system 3- Florida, prototype of suspension system 4 - Yugo 65 cl
D – acceleration direction	d=3	1 – X 2 – Y 3 – Z

Analysis of variance enabled the influence of external factors and measurement errors on experimental results in case when it is possible to combine one level of one factor with all levels of other factors [9].

Analysis of variance method is described in detail in [9]. Necessary expressions for analysis of three factors experiment are given in [9]. For four factors experiments, expressions are developed based on three factors experiment.

Degrees of freedom of factors are given in table 2, according to [9].

Table 2 Variance table of RMS accelerations

Excitatione	Degree of freedom	Sums of squares	Average square	v_0	C for V=95%
A	1	1.09424	1.094238	0.02979	254

B	2	6.318848	3.159424	0.08601	19.5
C	3	30.72168	10.24056	0.27879	8.53
D	2	5231.779	2615.889	71.2154	19.5
AB	2	1.602832	0.801416	0.02182	19.5
AC	3	5.728472	1.909491	0.05198	8.53
AD	2	2.563704	1.281852	0.03489	19.5
BC	6	10.40352	1.733999	0.04720	3.67
BD	4	5.470605	1.367765	0.03723	5.63
CD	6	8.91543	1.485905	0.04045	3.67
ABC	6	52147.73	8691.288	185.204	3.67
ABD	4	416.2613	104.0653	74.2886	5.63
ACD	6	23294.97	3882.495	54.2886	3.67
BCD	12	8993.058	749.4214	5.30219	2.30
ABCD	12	94947.54	7912.295	112.587	2.30
Error	288	10578.83	36.7328		
Sum	359				

According to results of dispersion analysis given in Table 2 the factor D (direction factor) effect is significant. In addition, the factorial effect of fore and aft factor interaction is significant.

In order to decrease inter factor interaction transformation of coordinates are conducted, [9]. Coordinates transformation by using of square root, logarithm or square values caused stronger inter factor interactions [15,16,47].

International standard ISO 2631/1 [7], as well older standard issues, recommended frequency weighting of rms accelerations. Experimental results are weighted according to [7,19] in order to obtain reliable data.

Spectral analysis of acceleration time series were performed. Acceleration power spectrums are weighted by multiplying with weighting factors W_k (vertical direction) and W_d (fore and aft and lateral directions) for sitting position according to ISO 2631/1 [7]. Based on obtained weighted power spectrums r.m.s. values of accelerations are determined. Analysis of variance procedure is repeated. Results are given in detail in [11,12] and are the same as well as obtained previously.

Normalized R.M.S. values of acceleration signals are analysed by variance method analysis, the same procedure applied in previous section. Results are given in Table 3. Conclusions are the same as well as in previous two cases.

Table 3. Variance table of normalized RMS accelerations

Excitation	Number of factor level	Sums of squares	Average square	v_0	C for V=95%
A	1	13.26153	13.26153	42.311024	254
B	2	3.796913	1.898457	6.057043	19.5
C	3	0.835625	0.278542	0.888689	8.53
D	2	16.99749	8.498748	27.115332	19.5
AB	2	0.287930	0.143965	0.459322	19.5
AC	3	1.010636	0.336879	1.074815	8.53
AD	2	0.533410	0.266705	0.850925	19.5
BC	6	1.404979	0.2341632	0.747100	3.67
BD	4	0.5207565	0.1301891	0.415370	5.63
CD	6	0.2034459	0.033908	0.108183	3.67
ABC	6	453.7496	75.62494	241.283043	3.67
ABD	4	65.9325	16.48313	52.589558	5.63
ACD	6	221.6583	36.94305	117.867134	3.67
BCD	12	148.273	12.35608	39.422184	2.30
ABCD	12	967.4673	80.62228	257.226074	2.30
Error	288	90.26733	0.313429	0.313430	
Sum	359				

Results can be analysed by application of regression test of significance. Method was described in detail in [64]. Elements given in Table 4 are determined according to [9]. Confirmation of factorial experiment by method of regression test of significance was given in Table 4.

Conclusions obtained by application of analysis of variance and regression test of significance are the same. Influential factor on acceleration level is direction factor *D*.

Regression test of significance method has advantage over analysis of variance method in easier calculation especially in factorial experiment with high level and number of factors. Application of previously method could not obtain analysis of inter factor relationships [9].

Further analysis is subordinate to type of factors. Analysis of variance is the same in both cases. Factor of direction has the most significance level and is confirmed by average values analysis.

In order to compare average values, in reference to determine direction of dominant loadings of passenger, Student's t-test is determined according to [9]:

$$t_0 = \frac{D}{s \sqrt{\frac{1}{r} \left(\frac{1}{m} + \frac{1}{n} \right)}}, \quad (1)$$

where are: s - standard error dispersion, r - number of repeated readings for the same factor combination, n and m - numbers of average values in comparing groups. Value D is:

$$D = \frac{\bar{x}_1 + \dots + \bar{x}_n}{n} - \frac{\bar{y}_1 + \dots + \bar{y}_m}{m}, \quad (2)$$

where are x_i and y_i are two compared groups of average values. Criterion has the same degree of freedom as well experiment error. Value v_0 is standard value and based on criterion $v_0 > v_{0table}$ group of higher average values can be determined, [9].

Number of repeated readings in experiment was $r=5$ and number of compared average values are $m=n=24$. According to table 2 value s is:

$$s = \sqrt{\text{Average square error}} = 6.06069.$$

For degree of freedom value 288 and confidence interval $\alpha=0.05$ i $t_{0table}=1.96$, determined values of t_0 can be compared:

$$\begin{aligned} t_0[x, y] &= 8.228392 & \ddot{X} > \ddot{Y}, \\ t_0[z, x] &= 233.0132 & \ddot{Z} > \ddot{X}, \\ t_0[z, y] &= 241.2416 & \ddot{Z} > \ddot{Y}. \end{aligned} \quad (3)$$

According to equation (3), the highest loading of human in operational conditions are in vertical direction and the lowest is in the lateral direction.

Conducted experiment is analyzed as factorial experiment, because all factor combinations could be arranged [64].

Analysis of variance and regression test of significance pointed out significant direction factor. Analysis showed that transformation of coordinates should not be performed, as well as acceleration weighting in order to determine the most influenced factor, [11,12,21], results are the same. Analysis of average values showed that dominant loadings are i vertical direction and the lowest is in lateral direction.

Table 4. Regression test of significance

Factor	m	t _j	SR(m,t _j)	SR(m')	SF	SG	v ₀	V _{0table}
A	3.9669083	0.0550678 -0.055066	5666.1834	5665.0227	1.160664	5786.8166	0.0718	254
B		-0.164235 0.1601642 4.07087e-3	5671.4072		6.384521	5781.5928	0.1971	19.5
C		-0.0151805 -0.2493305 -0.2169972 0.4815106	5695.8098		30.787086	5757.1902	0.6345	8.53
D		-2.5603766 -2.8286344 5.3890084	10896.835		5231.8118	556.165	1678.87	19.5

Assessment of linear dependence between two signals can be determined by correlation coefficient, according to [1]:

$$\rho_{xy} = \frac{\sigma_{xy}}{\sigma_x \sigma_y}, \quad -1 \leq \rho_{xy} \leq 1 \quad 4)$$

where are σ_x standard deviation of input signal, σ_y standard deviation of output signal, σ_{xy} covariance of signals x and y .

Correlation coefficients are determined according to (4) and are given in Table 5, are different from extreme values. There is both correlation between acceleration in vertical and longitudinal direction and correlation between vertical and lateral accelerations. There is nonlinear correlation between acceleration signals. Results are given in Table 5 in columns 7-9. Obtained results point out smaller correlation between signals. Comparison of correlation coefficients showed stronger relationship between vertical and longitudinal acceleration.

Coherence function that describes statistical couplings between two signals is analog to correlation coefficient. It is more convenient tool than correlation coefficient with respect to analysis of system behavior in frequency significant domain, [1].

Values of coherence function are in interval 0-1. Based on data given in figure 4 there is stronger statistically couplings between fore and aft acceleration and vertical acceleration than between lateral and vertical acceleration. It is obvious that there is nonlinear correlation between signals, [3].

Table 5 Correlation coefficients

σ_x	σ_y	σ_z	σ_{xy}	σ_{xz}	σ_{yz}	ρ_{xy}	ρ_{xz}	ρ_{yz}
0.021909	0.030954	0.080475	0.000321	-0.008141	0.006439	0.012342	-0.16314	0.15335
0.048247	0.092622	0.207435	0.007143	0.027635	0.02695	0.106859	0.276239	0.01945
0.048247	0.092622	0.207435	0.007143	0.027635	0.02695	0.106859	0.276239	0.01945
0.450209	1.008203	1.732715	-0.022318	0.291851	-0.028132	-0.033127	0.330439	-0.0218
0.128818	0.561031	0.493499	-0.009030	0.117296	0.021552	-0.033590	0.465214	0.04096
0.101608	0.24910	0.376176	0.027115	-0.008824	0.018481	0.170435	0.094527	-0.0288
0.030665	0.025234	0.106521	0.000417	0.021689	0.012679	0.014986	0.379494	0.24454
0.057712	0.057528	0.096853	-0.010524	0.032849	0.008958	-0.18264	0.439378	0.12009
0.085830	0.075939	0.315493	0.013744	0.074922	0.026792	0.170244	0.455296	0.17309
0.743727	0.802565	0.335762	-0.118843	0.851143	0.142046	-0.153824	0.538617	0.08653
0.562435	0.311502	0.133511	-0.0011183	0.308725	0.133236	-0.026717	0.356215	0.20657
0.384022	0.257761	0.621458	-0.027205	0.181111	-0.043076	-0.08647	0.370733	-0.1076
0.405643	0.265238	0.371269	0.005157	0.159862	0.000657	0.015721	0.411935	0.00209
1.002021	0.824650	1.399682	-0.086248	0.612796	-0.0990	-0.094031	0.512810	-0.0921
0.892577	0.775624	1.788532	-0.097902	0.732115	-0.022050	-0.117664	0.579439	-0.0187
0.076736	0.109851	0.131883	-0.064051	0.016619	-0.00711	-0.697623	0.165200	-0.0059
0.062012	0.068803	0.187060	-0.024304	0.013344	0.007064	-0.372084	0.117666	0.06558
0.025505	0.022215	0.092893	0.000579	-0.002728	0.011264	0.024340	0.247947	-0.0560
0.123422	0.340681	0.278213	-0.054883	0.055898	-0.008012	-0.267648	0.301654	-0.0260
0.054973	0.073076	0.165952	0.006817	0.025106	0.025157	0.0107563	0.262848	0.22848
0.123422	0.340681	0.278213	-0.054883	0.055898	-0.008014	-0.267648	0.301654	-0.0260
0.515318	0.348888	1.747677	-0.058049	0.475656	0.166879	-0.136904	0.501215	0.21371
0.269019	0.105881	0.457689	-0.046379	0.146154	0.034476	-0.274796	0.416518	0.15660
0.080283	0.103750	0.211660	-0.030203	0.012092	0.00137	-0.330932	0.092759	0.00922

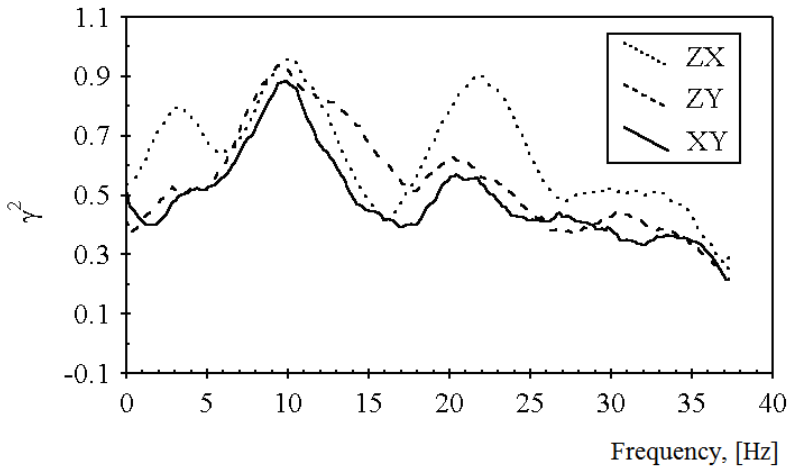


Figure 4 Coherence function between accelerations in for and aft and lateral directions and vertical directions

Loadings affected on human are analysed by Seat to head transfer function in three directions, figures 4, 5 and 6.

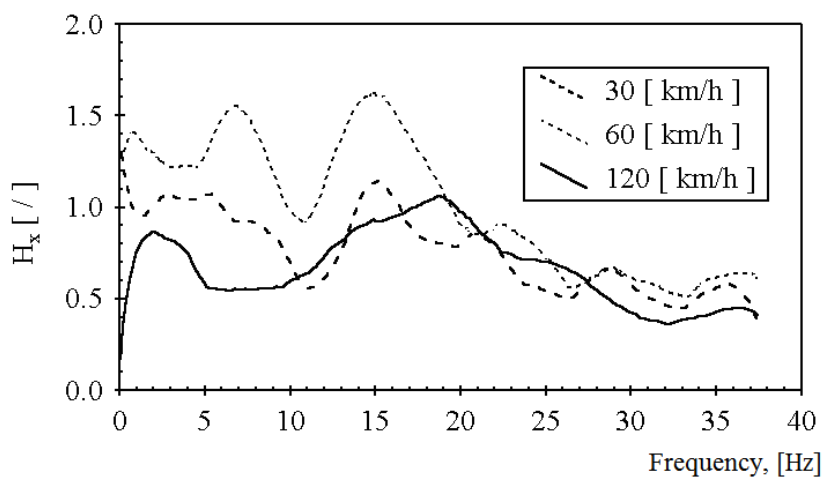


Figure 5 The influence of vehicle speed on transfer function of floor seat in fore and aft direction

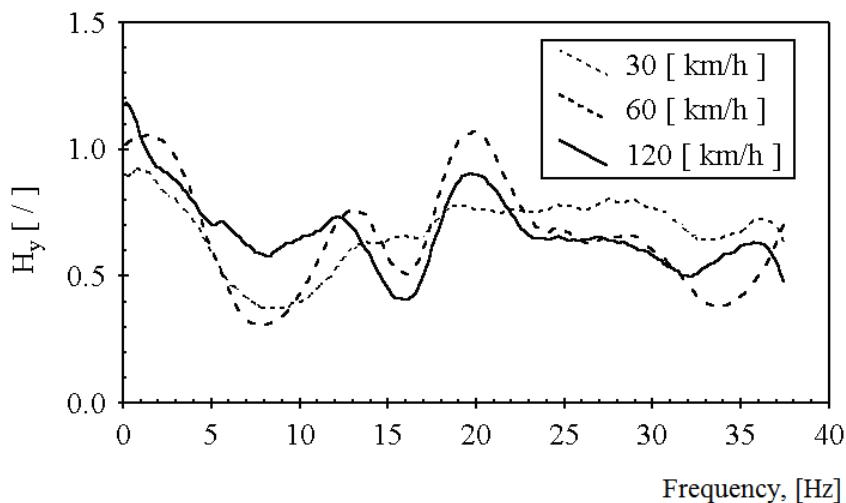


Figure 6 The influence of vehicle speed on transfer function of floor seat system in lateral direction

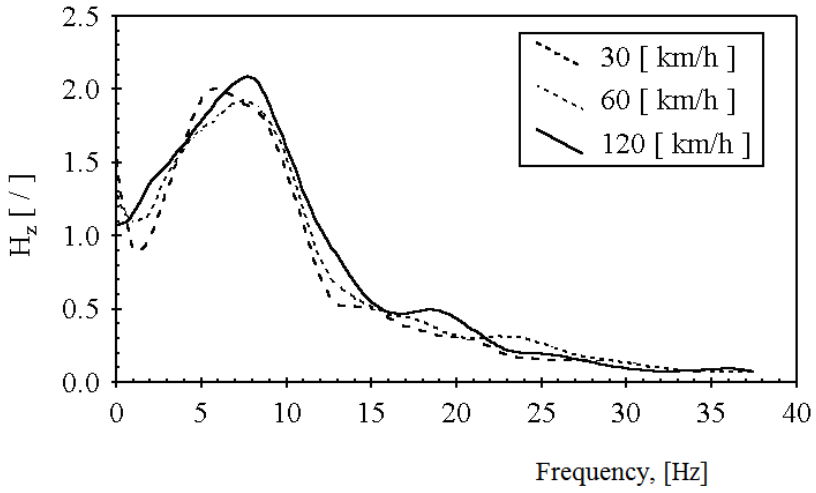


Figure 7 The influence of vehicle speed on transfer function of floor seat in vertical direction

Change of vehicle speed affected change of transfer function amplitude that indicated that system floor - seat is nonlinear in all directions [11].

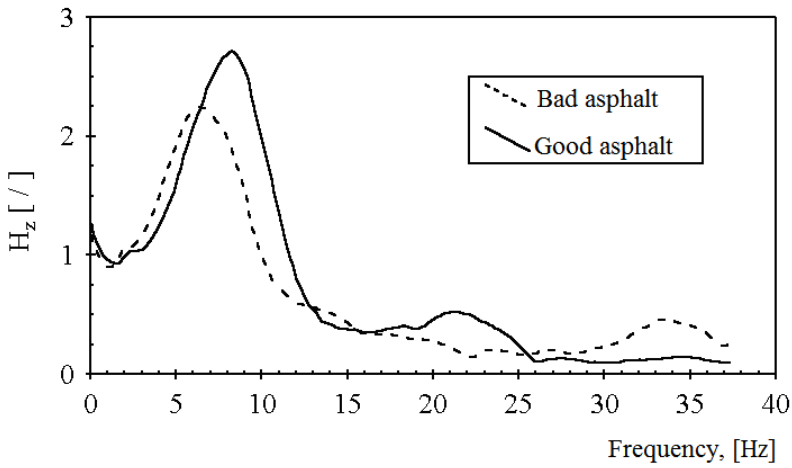


Figure 8 The influence of road surface on transfer function of floor seat system in vertical direction

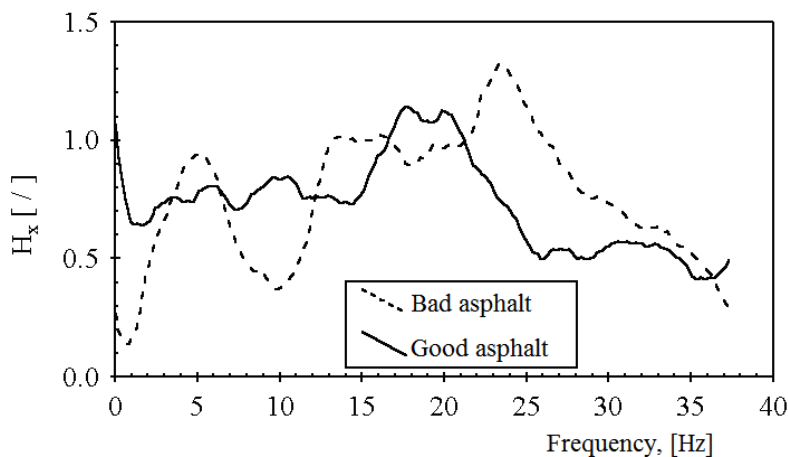


Figure 9 The influence of road surface on transfer function of floor seat system in fore and aft direction

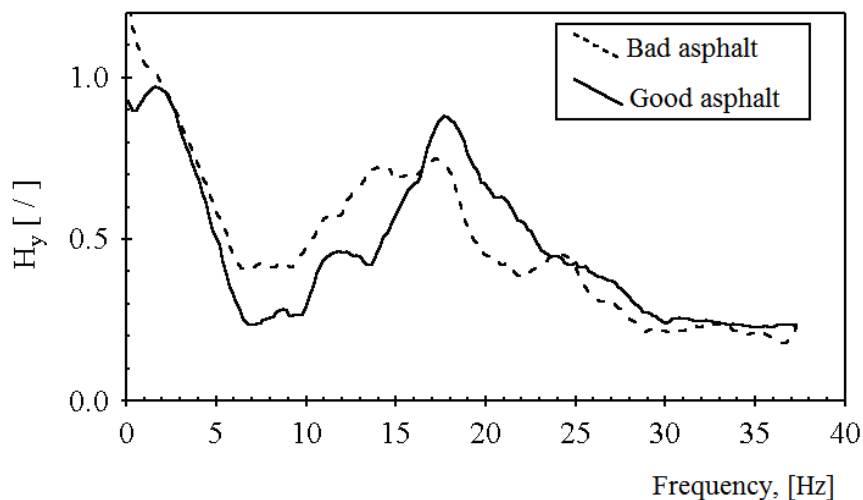


Figure 10 The influence of road surface on transfer function of floor seat system in lateral direction

The influence of road surfaces on transfer function of floor seat system is given in figures 8 - 10 (good and bad asphalt) in all three directions. Presented diagrams pointed out on system nonlinearity.

In order to determine couplings between acceleration signals in vertical and lateral and fore and aft directions partial coherence function is determined. Field investigations were performed in order to define dominant loading directions and to define excitations direction for further research.

If system has two input $x_1(t)$ and $x_2(t)$ and one output (z) than partial coherence function $\gamma_{2,y,1}$ represents statistical correlation between signals x_2 and y , when linear effects of input signal x_1 are removed from both signals. Partial coherence function is:

$$\gamma_{2y,1}^2 = \frac{|S_{2y,1}|^2}{S_{22,1}S_{yy,1}}, \tag{5}$$

where are:

- $S_{22,1}$ and $S_{yy,1}$ conditional autospectrums of x_2 and y signals when linear effects of x_1 signal are removed from x_2 and y signals and
- $S_{2y,1}$ conditional cross spectrum of x_2 and y signals when linear effect of x_1 signal are removed [1].

When input signals x_1 and x_2 , are acceleration signals in fore and aft direction x and lateral direction y , and output signal z is acceleration signal in vertical direction, partial coherence function between z and y signals, when the linear effects of signal x is removed is:

$$\gamma_{yz,x}^2 = \frac{|S_{yz,x}|^2}{S_{yy,x}S_{zz,x}}. \tag{6}$$

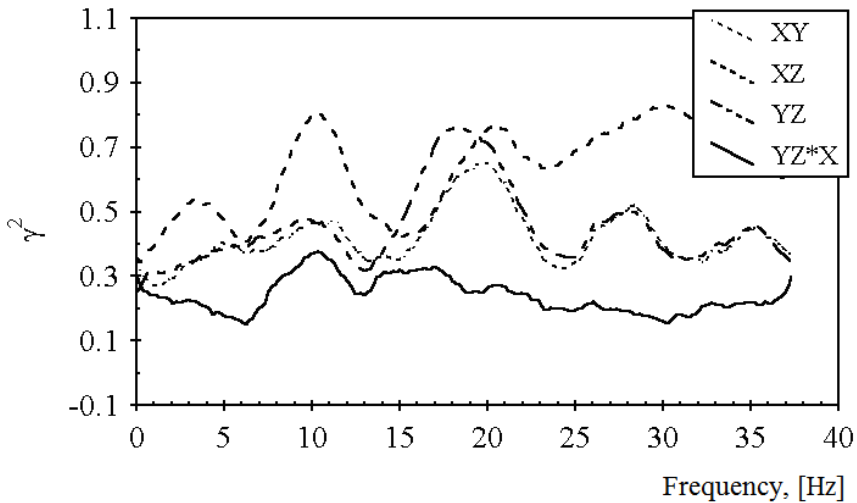


Figure 11 Ordinary coherence function and partial coherence function

According to diagram given in figure 11, there is stronger correlation between accelerations in fore and aft and vertical direction than accelerations in lateral and vertical direction. Diagrams given in figure 11 showed that low level of partial correlation between acceleration in vertical and lateral direction (maximum values are up to 0.4 when linear effect of signals in fore and aft directions are removed).

Performed analysis showed that dominant oscillatory loads of passengers are in vertical and fore and aft directions and observed system is non-linear in all three directions.

Results obtained in field experiments are starting point for further laboratory investigations of passenger cars ride comfort. The broadband random excitations affect on human body in sitting position and will be investigated in further laboratory experiments.

3. 2 HEAVY VEHICLES

According to average r.m.s. values of accelerations in extreme operational conditions and maximal values of acceleration magnitudes, crest factor is less than 9, which caused to apply assessment methods based on r.m.s. accelerations values, [7].

Root mean squares values of accelerations are determined from 1/3 octave spectrums with constant relative bandwidth. R.M.S. values of vertical and horizontal (fore and aft and lateral) accelerations are compared with equivalent comfort curve of 8 hours, according to standard ISO 2631/85, and r.m.s. values of accelerations in vertical and horizontal directions on steering wheel are compared with equivalent comfort curves for 4-8 hours according to standard ISO 5349/79. Equivalent comfort curves for 4-8 hours are adopted as well reference. Vibration measured on the steering wheel are not considered in this paper.

Spectrums of r.m.s. accelerations on the seat are given in figures 12 - 13. Accelerations are measured on seat of loaded truck 49 10H driven on bad asphalt road with speed 70 km/h.

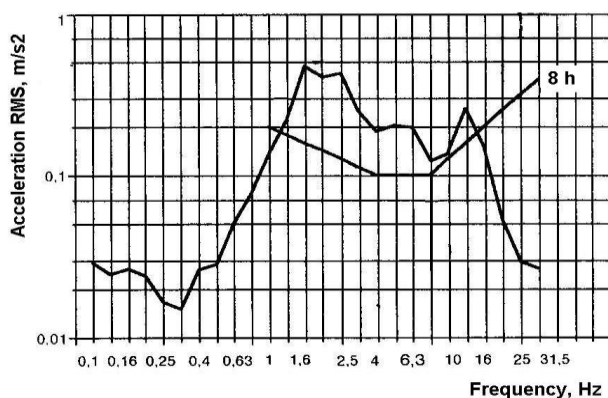


Figure 12 Spectrum of vertical accelerations measured on seat, respect to equivalent comfort curves for 8h, according to ISO 2631/85

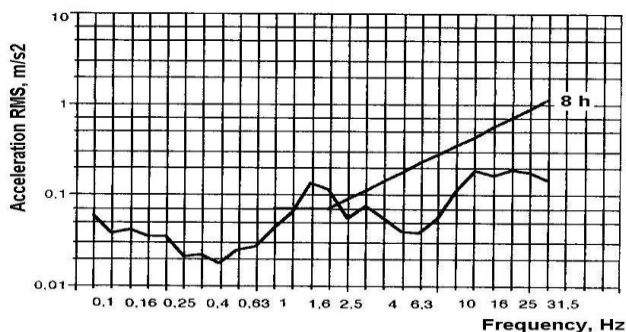


Figure 13 Spectrum of fore and aft accelerations measured on seat, respect to equivalent comfort curves for 8h, according to ISO 2631/85

Analysis of vertical accelerations spectrums showed significant spectrums density in frequency region between 2 and 8 Hz, where are human body resonances. Power spectrums are highest in vertical directions and the lowest in horizontal (lateral) directions. Spectrum

of vertical acceleration measured on the floor has more power than acceleration spectrums measured on the seat and steering wheel.

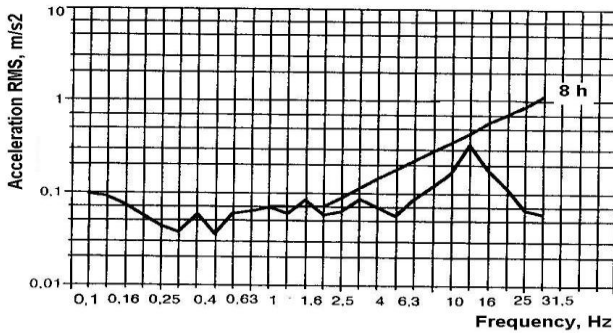


Figure 14 Spectrum of lateral accelerations measured on the seat respect to equivalent comfort curves for 8h, according to ISO 2631/85

Vehicles used in this investigation do not satisfy requirements of standard ISO 2631/8 for equal comfort curves for 8 hours in vertical direction and satisfy requirements for horizontal (fore and aft lateral) vibrations.

In order to determine dominant oscillatory loads of users of duty vehicle, analysis of variance method were applied, the same method applied on passenger cars.

Performed experiment has four influenced factors, described in table 6.

Table 6 Experimental factor

Factor	Factor level	Elements
A-road	a=2	1-good asphalt 2-bad asphalt
B-loading	b=2	1-loaded 2-unloaded
C-vehicle model	c=3	1-4910H 2-7912 3-110E18
D-direction	d=3	1-x 2-y 3-z

Results of performed analysis are given in table 7.

Table 7. Variance table of RMS accelerations

Excitation	Degree of freedom	Summs of squares	Average square	v_0	C for $v=95\%$
A	1	0.61	761	0.0554	3.90
B	1	0.84	0.84	0.006	3.90
C	2	0.30	5.15	0.037	3.06
D	2	2794	1397	10.18	3.06
AB	1	258	6258	45.61	3.90
AC	2	6220	3110	22.66	3.06
AD	2	6216	3108	22.66	3.06
BC	2	6218	3109	22.66	3.06

BD	2	6218	3109	22.66	3.06
CD	4	6226	1556	11.34	2.43
ABC	2	-12468	-6234	-45.4	3.06
ABD	2	-12486	-6243	-45.5	3.06
ACD	4	-15188	-3797	-27.66	2.43
BCD	4	-12456	-3114	-22.69	2.43
ABCD	4	-3460	-865	-6.30	2.43
Error	144	19757	1372		
Summ	179	2856			

Degree of freedom was 144 and confidence interval was $\alpha=0.05$ and $t_{0tablično}=2.62$ [12]. Obtained values of t_0 can be mutually compared. Results are:

$$t_0[z, x] = 18.86 > 2.62 \rightarrow \ddot{z} > \ddot{x},$$

$$t_0[z, y] = 20.14 > 2.62 \rightarrow \ddot{z} > \ddot{y}. \quad (7)$$

The highest loading is in vertical direction and the lowest loading is in lateral direction.

Performed experiment is analysed as factorial. The main condition for factorial experiment, possibility of mutual combination of all levels of all factors, was satisfied, [9].

Analysis of coherence functions between accelerations in three directions was performed.

Partial results of coherence function analysis are presented in figures 16 -19. Coherence functions between accelerations measured on the floor and seat of loaded duty vehicle Rival 4910.H driven on bad asphalt road are given.

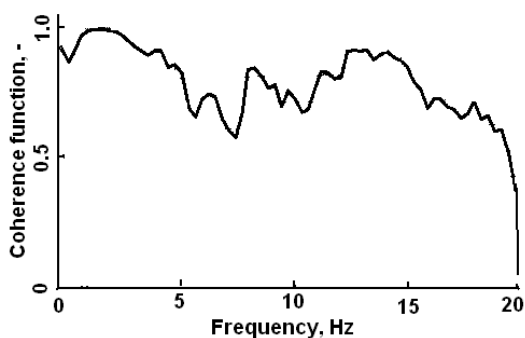


Figure 15 Coherence function between measured accelerations on the floor and seat, Z-direction

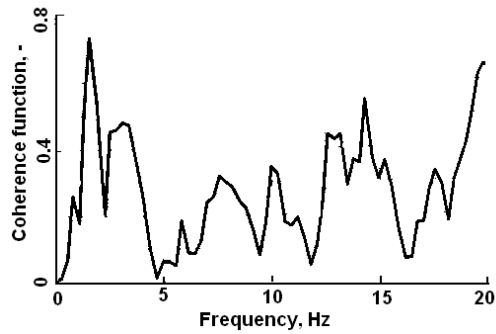


Figure 16 Coherence function between accelerations measured on the floor and seat, X-Y-direction

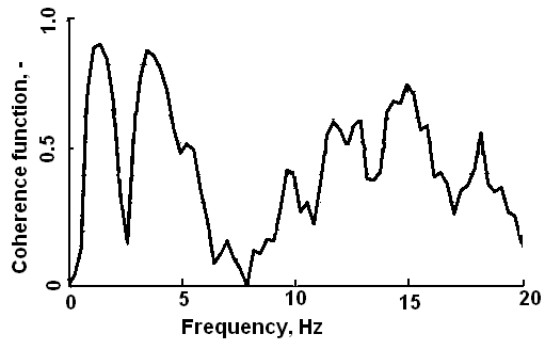


Figure 17 Coherence function between accelerations measured on the seat, Z-X-direction

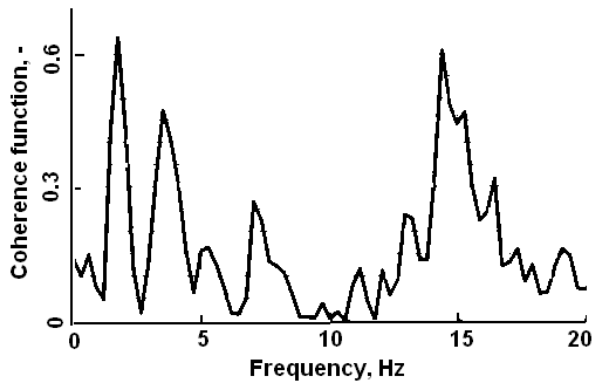


Figure 18 Coherence function between accelerations measured on the seat, Z-Y-direction

According to figures 16-19, there is higher level of linearity and mutual dependence between vertical and fore and aft accelerations than between vertical and lateral accelerations. The highest mutual dependence between vertical and fore and aft accelerations are in frequency region between 2 and 8 Hz and between 12 and 16 Hz.

Analysis of variance and coherence function analysis showed that dominant vibratory loads of trucks are in vertical and fore and aft directions.

4. CONCLUSIONS

Based on performed experimental investigation conclusions are:

- developed experimental methodology enables obtaining reliable results about factor effects on vibratory loads of human in motor vehicle (passenger car, truck),
- dominant vibratory loadings of human in passenger car are in vertical and fore and aft directions,
- dominant vibratory loadings of human in truck are in vertical and lateral directions,
- field experiment results obtained further laboratory investigations.

ACKNOWLEDGEMENT

Paper is result of project TR35041 financially supported by Ministry of education and science of Republic of Serbia.

References

- [1] Bendat J. S. and Piersol A.G.: Engineering Applications of Correlation and Spectral analysis, John Wiley & Sons, New York, 1980.
- [2] British Standard Institution: Measurement and evaluation of human exposure to whole body mechanical vibration and repeated shocks, BS 6841, London, 1989.
- [3] Corbridge C. and Griffin M. J.: Vibration and comfort: vertical and lateral motion in the range 0.5 - 5.0 Hz, Ergonomics, vol.29, No.2, 1986, pp. 249-272.
- [4] Giuliano F. and Bucco A.: A road test procedure for definition of the vibratory mission of automotive seats, 3rd International conference Vehicle comfort and ergonomics, Bologna, 1995
- [5] Griffin M. J., Whitham E. M. and Parsons K. C: Vibration and comfort I: Translational seat vibration, Ergonomics, vol. 25, No. 7, 1982, pp 603-630
- [6] Griffin M. J.: Handbook of Human Vibration, Academic Press, London, 1990.
- [7] International Standardization Organization: Guide for the evaluation of human exposure to whole body vibration, ISO 2631/1, Geneva, 1997.
- [8] Khatib A. E., Guillon F. and Domont A.: Vertical transmission through the lumbar spine of the seated subject-first results, Journal of Sound and Vibration, Vol. 215, No. 4, 1998.
- [9] Kostić M.: Statistical methods of analysis with computational approach, in Serbian, Naučna knjiga, Beograd, 1988.
- [10] Latherwood J. D., Dempsey T. K. and Clevenson S. A.: A Design Tool for Estimating Passenger Ride Discomfort Within Complex Ride Environments; Human Factors, vol.22, No.3, 1980, pp 291-312
- [11] Lukić J.: Ride comfort parameter identification of passenger cars, Ph.D. Thesis, University of Kragujevac, Faculty of Mechanical engineering, Kragujevac, 2001.
- [12] Milić Ž.: Ph.D. Ride comfort parameters of heavy vehicles, PhD Thesis, University of Kragujevac, Faculty of Mechanical engineering, Kragujevac, 2001.

- [13] Osborne D. J., Boarer P. and Heath T. O.: Variations in response to whole body vibration.. Intensity dependent effects, *Ergonomics*, vol. 24, No. 7, 1981, pp 523-530
- [14] Osborne D. J., Heath T. O. and Boarer P.: Vibration in human response to whole body vibration, *Ergonomics*, Vol. 24, No. 4, 1981, pp 301-313
- [15] Paddan G. S. and M. J. Griffin: The transmission of translational seat vibration to the head - I. Vertical seat vibration, *Journal of Biomechanics*, Vol. 21, No 3, 1998, pp 191-197.
- [16] Paddan G. S. and M. J. Griffin: The transmission of translational seat vibration to the head - II. Horizontal seat vibration, *Journal of Biomechanics*, Vol. 21, No 3, 1998, pp 199-206.
- [17] Wheeler A., Ganji A.: *Introduction to Engineering experimentation*, Prentice Hall, 2010.
- [18] Simić D.: *Beitrag zur Optimierung der Schwingungseigenschaften des Fahrzeuges Physiologische Grundlagen des Schwingungskomfort*, Doctor Disertation, TU Berlin 1970.
- [19] Simić D., Robbins D. R.: General human vibration: International standard ISO 2631, state and research trends, *MVM*, No. 58/59, Vol X, Kragujevac, 1984, pp. 452-473,
- [20] Simić D.: The influence of complex mechanical oscillations on human, *MVM*, 37/38, Vol VII, Kragujevac, 1981, pp.34-46.
- [21] Demeć M., Lukić J., Milić Ž.: Some aspects of the investigation of random vibration influence on ride comfort, *Journal of sound and vibration*, Vol. 253, No 1, 2002, pp. 109-129

MVM Editorial Board
University of Kragujevac
Faculty of Engineering
Sestre Janjić 6, 34000 Kragujevac, Serbia
Tel.: +381/34/335990; Fax: + 381/34/333192
www.mvm.fink.rs